Check for updates

Heavy metal adsorption by graphene oxide modified with 5-amino-3(2-thienyl)pyrazole using central composite design/response surface methodology (CCD/RSM)

Mobina Alimohammady,[a] Mansour Jahangiri, [ID] *[a] Masoud Salavati-Niasari [ID] *[b] and Aseel M. Aljeboree[c]

In this study, graphene oxide (GO) was chemically functionalized with 5-amino-3(2-thienyl)pyrazole (5-ATP), introducing oxygen-, nitrogen-, and sulfur-containing groups, to enhance adsorption performance and develop a multifunctional adsorbent (5-ATP-GO) for efficient removal of Cd(II), Hg(II), and As(III) from aqueous solutions. The GO and 5-ATP-GO composites were characterized by Fourier transform infrared spectroscopy, field-emission scanning electron microscopy, thermogravimetric analysis, X-ray diffraction, energy-dispersive X-ray spectroscopy, Brunauer–Emmett–Teller analysis, Raman spectroscopy, and zeta potential analysis. The performance of 5-ATP-GO for heavy metal removal was evaluated by design of experiment to optimize operational parameters and assess adsorption capacity. Central composite design/response surface methodology analysis was applied for the optimization of adsorbing conditions, (*i.e.*, pH, initial metal ion concentrations, and adsorbent dosage). Furthermore, analysis of variance revealed that quadratic equations well predicted experimental data with an R^2 value of >0.99 and a *p*-value of <0.05. Experimental optimization variables were a pH of 7.25–8.55, an initial metal ion concentration of 43.45–49.66 mg L^{-1}, and an adsorbent dose of 10–10.50 g L^{-1}. Results showed that most of the adsorption occurred within the first 30 minutes, during which only 0.2 g L^{-1} of 5-ATP-GO successfully removed 79.8% of Hg(II), 86.5% of Cd(II), and 75.1% of As(III) ions from the solution. These rapid kinetics were further supported by high adsorption capacities of 213.5 mg g^{-1} for Hg(II), 280.1 mg g^{-1} for Cd(II), and 450.95 mg g^{-1} for As(III), underscoring the superior uptake potential of 5-ATP-GO toward toxic metal ions. Furthermore, adsorption kinetics and isotherm studies revealed that the data were well fitted to the pseudo-second-order kinetic model and Freundlich isotherm, indicating that the adsorption process follows a heterogeneous chemisorption mechanism. Finally, comparative experiments with pristine GO and other conventional adsorbents confirmed the superior removal efficiency and enhanced performance of the 5-ATP-GO composite.

1 Introduction

The increasing heavy metal concentration in the atmosphere caused by rapid population growth and industrialization raises serious global concerns because of the toxicity and bioaccumulation of these metals at extremely high levels. The pollution caused by metal ions can be reduced through electrolysis, ion exchange, precipitation, adsorption, and membrane separation. The electrolysis method, through the process of the redox reaction, removes heavy metal ions from water using direct current, but this method usually has the disadvantage of high energy consumption. Precipitation is the simplest method and is often performed *via* the reaction of heavy metal ions with functional groups such as sulfide, ferrite, and hydroxide in water. The method of ion exchange provides several benefits, including affordability, uncomplicated equipment, ease of operation, and minimal usage of organic solvents. However, it has some disadvantages, such as a lengthy production cycle, occasional substandard product quality, and significant pH variations during the production process. The separation of heavy metal ions by membranes involves selecting a proper membrane that will inhibit the passageway of metal ions, but membrane rigidity is low and simply congested. Moreover, many traditional water treatment technologies lack

[a]Faculty of Chemical, Petroleum and Gas Eng., Semnan University, P.O. Box 35196-45399, Semnan, Islamic Republic of Iran. E-mail: mjahangiri@semnan.ac.ir; Fax: +982333654120; Tel: +982331532477

[b]Institute of Nano Science and Nano Technology, University of Kashan, P. O. Box. 87317-51167, Kashan, Iran. E-mail: salavati@kashanu.ac.ir; Fax: +98 31 55913201; Tel: +98 31 55912383

[c]Department of Chemistry, College of Sciences for Girls, University of Babylon, Hilla, Iraq

acceptable efficiency in removing toxic metal ions, especially at the trace level. To solve these problems, the adsorption technique, with a low price, modest process, and great efficacy, was established as a useful method to be applied alone or in combination with typical methods.[1–5] Adsorption is a widely observed phenomenon that occurs at the interface of solids and liquids. In the handling of wastewater, adsorbents with large specific surface areas are frequently applied to eliminate ions of heavy metals from liquid mixtures. The adsorption process has been instituted to be a useful procedure that operates efficiently even at low concentrations, requires less operation time than alternative methods, and incurs lower costs.[6–8] Nevertheless, surface absorption with great capability at a marketable level and on a large scale does not work well. Therefore, the appropriate worthy adsorbent plans have been associated with the challenges of economic justification.[9,10] Thus far, silica nanoscale compounds and activated carbons are the most prosperous adsorbents commercially accessible.[11–13] However, these methods suffer from issues such as the absence of selectivity, great budget, inflexibility, laborious production, extensive energy usage, and the application of harmful materials and their disposal. Developing new adsorbents that are chemically versatile and can use waste or natural materials such as graphite, fly ash, starch, chitosan, clays, and zeolites is a promising method to overcome the restrictions. This approach promotes green production and sustainable matter, making it an ideal solution.

Among these materials, graphene is a remarkable material that has a unique two-dimensional structure. It can be manufactured on a large scale from graphite and has a vast surface area. Moreover, its chemical properties can be adjusted, and it can be designed in various three-dimensional shapes. Because of these characteristics, graphene is an excellent adsorbent for removing metal ions.[14,15]

Researchers have studied various methods of using graphene materials including GO, pristine graphene, and reduced graphene oxide (rGO) composites with polymers and nanoparticles. These methods have been applied in different three-dimensional composite forms, including foams, hydrogels, membranes, and aerogels.[16] By comparing different graphene composites, GO having a large density for various oxygen (O) functional parts such as carboxyl, lactone, and phenol by considerable electron-donating capability and binding affinity to metal ions has made an interesting option.[17] Moreover, it is possible to modify the O functionalities of GO by attaching specific groups containing phosphorous, nitrogen, and sulfur. This covalent attachment opens up new possibilities for designing advanced adsorbents that exhibit high selectivity and capacity to absorb heavy metals.[18] Alimohammady *et al.* employed this idea to produce a 3-aminopyrazole-GO adsorbent *via* the reaction between the amino group of 3-aminopyrazole and the hydroxyl and carboxyl groups on GO, indicating adsorption capacities (q_{exp}) for cadmium, mercury, and arsenic of 98.1, 82.3, and 42.3 mg.g^{-1}, respectively.[19] Moreover, they prepared 3-amino-5-phenylpyrazole-GO by reacting 3-amino-5-phenylpyrazole with carbonyl groups on GO *via* a substitution reaction. The results showed that this adsorbent outperformed

previous work, with q_{exp} values of 45.9, 84.6, and 99 mg g^{-1} for arsenic, mercury, and cadmium, respectively.[20] Furthermore, extensive research has been conducted to functionalize GO with molecules including sulfur and nitrogen groups owing to their great attraction toward heavy metals, which is endowed by their free valence electrons.[21–24]

The innovation of the article is as follows: if we look at the articles,[1–87] it can be seen that not much work has been done in the field of simultaneous removal of heavy metal ions including mercury, arsenic and cadmium from aqueous environments with the new adsorbent made in the present research (5-amino-3(2-thienyl)pyrazole-modified graphene oxide, 5-ATP-GO), and there is a need for further studies. The innovative functionalization of GO with 5-ATP provides a high density of active sites, enhancing the selectivity and adsorption capacity. Furthermore, the systematic optimization *via* Response Surface Methodology (RSM) renders methodological robustness, ensuring precise control over removal efficiency under different conditions. These advancements collectively demonstrate a significant leap in addressing critical challenges in water pollution mitigation compared to existing approaches. Therefore, the present work aims to remove the ions of three heavy metals, namely mercury, arsenic and cadmium ions, polluting the water environment with a new adsorbent made, and the design of the experiment is presented herein.

The objective of this research is to develop additional functional groups, specifically amino and sulfur, and incorporate them with the oxygen groups of GO to create a 3D graphene compound with diverse surface chemistries that enhance the binding performance of heavy metals such as arsenic, mercury, and cadmium. This study also introduces a straightforward approach for the surface functionalization of graphene oxide, leveraging the high density of oxygen-, sulfur-, and amine-containing materials to improve the adsorbent's performance, thus providing an effective and economically efficient method for heavy metal removal technologies. The methodology, illustrated in Fig. 1, involves the covalent attachment of 5-ATP to the carboxyl groups of GO *via* substitution reactions to form amide bonds. The characteristics of the 5-ATP-GO composite were extensively evaluated using various techniques including Fourier transform infrared (FTIR) spectroscopy, field-emission scanning electron microscopy (FE-SEM), thermogravimetric analysis (TGA), X-ray diffraction (XRD), energy-dispersive X-ray (EDX) spectroscopy, Brunauer–Emmett–Teller (BET) analysis, Raman spectroscopy, and zeta potential (ZP) analysis to determine its chemical, thermal, and structural properties. The prepared adsorbent was utilized to extract As(III), Hg(II), and Cd(II) ions from the solution, with sonication employed during the adsorption processes to enhance the mass transfer and reduce the adsorption time. Additionally, the study aims to optimize the adsorption process by examining the effects of initial pH, adsorbent dose (m, mg), and initial concentration of heavy metal ions (C_0, mg L^{-1}) through central composite design (CCD) under RSM to refine the variables influencing adsorption capacity (q). Moreover, this research analyzes the kinetics, competitive adsorption, equilibrium isotherms, and heavy metal desorption from the adsorbents. Finally, to evaluate the 5-
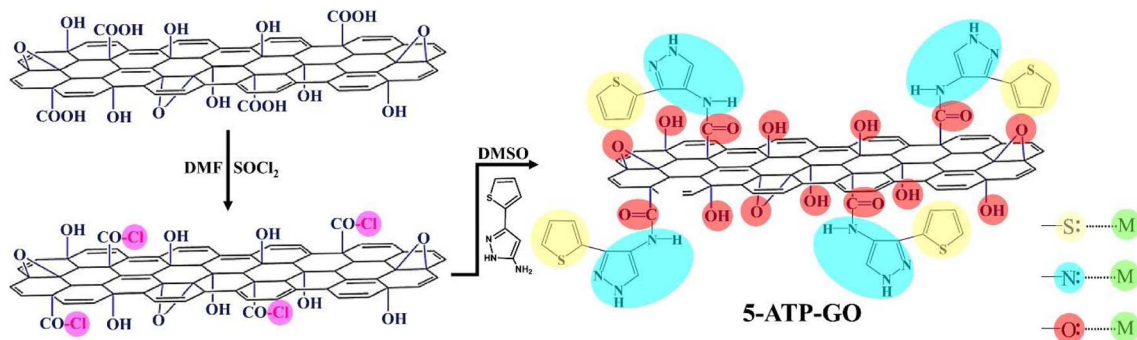
Fig. 1 Scheme of GO modification by 5-amino-3(2-thienyl) pyrazole.

ATP-GO efficiency under real conditions, the adsorbent's performance was tested using Caspian Sea water (Iran), contaminated with Cd(II), and compared with GO and commercial activated carbon.

These findings highlight the potential application of the novel 5-ATP-GO adsorbent synthesized in the present work in various industrial areas, especially wastewater from chemical, metal and steel, mining, electroplating industries, *etc.*, where efficient removal of heavy metals such as arsenic, mercury and cadmium is essential. By addressing multiple pollutants in a single process, this study contributes to more effective and sustainable wastewater treatment solutions, ultimately enhancing compliance with environmental conventions and reducing industrial impacts on aquatic environments.

2 Laboratory part

2.1 Chemicals and materials

GO was provided by Iran-Nano Science Co. Ltd (Iran). The chemicals, namely, 99% thionyl chloride (SOCl$_2$, Merck), tetrahydrofuran (C$_4$H$_8$O, THF, Merck), *N*,*N*-dimethylformamide (HCON(CH$_3$)$_2$, DMF, Merck), dimethyl sulfoxide (C$_2$H$_6$OS, DMSO, Merck), cadmium nitrate tetrahydrate (Cd(NO$_3$)$_2$·4H$_2$O, Merck), arsenite (NaAsO$_2$·7H$_2$O, Sigma-Aldrich), mercury(II) chloride (HgCl$_2$, Merck), and 96% 5-amino-3(2-thienyl)pyrazole (C$_7$H$_7$N$_3$S, Sigma-Aldrich) were used. Double-distilled water was used in this work. 5-ATP-GO was synthesized according to Alimohammady *et al.*'s method.[19,20,37–39] The typical procedure is presented in section 2.2 and Fig. 1.

2.2 Preparation of functional 5-ATP-GO

5-Amino-3(2-thienyl)pyrazole-modified graphene oxide (5-ATP-GO) was synthesized according to Alimohammady *et al.*'s method.[19,20,37–39] The typical procedure is presented in Fig. 1. First, 250 mg of GO was dispersed in 40 mL of SOCl$_2$ and 1 mL of DMF to obtain a solution. This solution was agitated for 48 h underneath a reflux process at 70 °C. Afterwards, the remaining SOCl$_2$ was detached by reduced pressure distillation to produce the acyl chloride-functionalized GO (GO-COCl). GO-COCl was stirred with 400 mg of 5-amino-3(2-thienyl)pyrazole in 20 mL of DMSO solvent and the solution was mixed at 100 °C for 96 h. Next, the solution was cooled to room temperature, filtered and washed exhaustively with ethanol, DMF, and THF solvents.

Subsequently, the black residuals were dehydrated at room temperature for 8 h under vacuum conditions.

2.3 Characterizations

The prepared solid materials were examined using diverse techniques such as Fourier transform infrared (FTIR) spectroscopy (Nicolet 6700 Thermo-Fisher), thermogravimetric analysis (TGA, Mettler-Toledo, Switzerland), X-ray diffraction (XRD, 600 Miniflex, Rigaco, Japan), field-emission scanning electron microscopy (FE-SEM, Quanta 450, FEI, USA), energy-dispersive X-ray spectroscopy (EDX, MIRA3 TESCAN, Czech Republic), Brunauer–Emmett–Teller (BET, Belsorp-mini II, Japan) surface area analysis, Raman spectroscopy (Takram P50C0R10 with 532 nm Nd: YAG laser, Japan), and zeta-potential (ZP, Malvern, Nano ZS Zen3600, UK). Moreover, a furnace atomic absorption spectroscopy instrument (FAAS, GF-AAS, PerkinElmer AAS 900H, Waltham, MA, USA) was exploited to measure the remaining metal ion concentration

Table 1 CCD experimental conditions for the elimination of As(III), Cd(II), Hg(II) by GO and 5-ATP-GO

Run	pH	m (mg)	C_0(ppm)
1	4	20	50
2	4	10	20
3	7	23.5	35
4	7	15	35
5	4	20	20
6	4	10	50
7	10	10	20
8	7	15	35
9	7	15	35
10	7	15	35
11	2	15	35
12	10	20	20
13	12	15	35
14	7	6.6	35
15	7	15	60
16	10	20	50
17	7	15	35
18	10	10	50
19	7	15	35
20	7	15	10

^{a} m: Dose of Adsorbent (mg). ^{b} C_0: Early metal ion concentrations (ppm).

after the uptake processes. For quantification of the residual concentrations of Cd(II), Hg(II), and As(III) after the adsorption process, a graphite furnace atomic absorption spectrometer (GF-AAS, PerkinElmer AAS 900H, USA) equipped with appropriate hollow cathode lamps was used. Cadmium was measured using standard GF-AAS at a wavelength of 228.8 nm. Mercury was determined *via* the cold vapor AAS technique at 253.7 nm, and arsenic (As(III)) was measured using hydride generation AAS at 193.7 nm. All measurements were performed in triplicate to ensure the accuracy and reproducibility.

2.4 Adsorption studies

To evaluate the ability to adsorb cadmium, arsenic, and mercury, we followed the design of experiments (DOE) table. A 50 mL working solution of each heavy metal was prepared for the adsorption experiments, with the initial metal ion concentration, pH, and adsorbent dosage precisely defined based on the experimental design. The specific conditions for each run are detailed in Table 1. Sonication was applied to the solution for 2 hours at RT (20–25 kHz, 60 W) to ensure uniform mixing and dispersion of the 5-ATP-GO adsorbent. This process enhances the interaction between the adsorbent and metal ions by breaking up graphene oxide agglomerates and increasing access to active adsorption sites, thereby improving the overall efficiency.[26–30] The whole adsorption experiment was conducted by applying 5-ATP-GO in triplicate with a control running in parallel (without adsorbent). The pH of the solution was adjusted with hydrochloric acid (HCl, 0.1 N) and sodium hydroxide (NaOH, 0.1 N) before adsorption. Following the progression of adsorption, the samples were centrifuged (6000 rpm; 10 min) and filtered to extract the supernatant out of the residual heavy metal solution. The residual amount of heavy metal in the collected liquid sample was specified by GF-AAS.

The amounts of adsorbed metal ions (mg) per gram of adsorbent (q_t, mg g^{-1}) and the efficiency of mass removal (R_t, %), at a known tense, t, were calculated by the subsequent relationships:

$$q_t = (C_0 - C_t) \times V\, m^{-1}; \quad R_t = (C_0 - C_t) \times 100/C_0 \qquad (1)$$

where C_0 and C_t are heavy metal values at the start and time t (mg L^{-1}), and V and m symbolize the solution volume (L) and mass of adsorbent (g), respectively.

The role of adsorption variables, namely C_0, m, and pH, in the elimination of heavy metals was examined. In addition, to achieve the highest removal efficiency, experimental condition optimization was tested through the CCD, in which factors are examined at 5 stages (+α, +1, 0, −1, and −α), so that a second-

degree model can be used. CCD is fundamentally distinguished by 3 tasks, *i.e.* 2n factorial, 2n axial, and 6 center runs, and n represents the number of causes.[31]

In this research, CCD is carried out with 6 axials, 8 factorial points, and 6 duplicates at the central point (20 tests). For arithmetical computations,[32–36] parameter X was hinted like X_i as follows:

$$X_i = (X_{actual} - X_{center})/(X_{center} - X_{min}) \qquad (2)$$

Each trial range of parameters and its corresponding level in the adsorption process of Hg(II), Cd(II), and As(III) are presented in Table 2.

To define a way that the system behaves, a tentative quadratic equation was used. The equation consists of square, linear, and linear–linear expressions to determine the condition that is the best.[32–36] Based on a quadratic polynomial (eqn (3)), the answer as a purpose of several variables' interactions can be determined:

$$Y = \beta_0 + \sum_{i=1}^{3} \beta_i X_i + \sum_{i=1}^{3} \sum_{j=i+1}^{3} \beta_{ij} X_i X_j + \sum_{i=1}^{3} \beta_{ii} X_i^2 \qquad (3)$$

where X_j and X_i are independent quantities; Y represents the response; β_0 is a constant; β_i, β_{ij}, and β_{ii} are the linear, linear interaction, and the quadratic outcome caused by the input factor, respectively. To analyze the experimental data, the Design-Expert 8.0.7.1 software was used along with ANOVA (analysis of variance). Through this, the key effects along with the interaction between the responses and parameters were determined.[19,37–39] The coefficient of correlation (R^2) was performed to evaluate the quality of eqn (3) and the statistical significance was determined using F-test.

2.5 Equilibrium study

All adsorption experiments in the kinetic and isotherm studies were conducted under the optimized conditions obtained from the CCD-based experimental design, including the optimum pH, adsorbent dosage, and initial metal ion concentration. Each experimental condition was tested in triplicate to enhance statistical robustness and minimize experimental error.

2.5.1 Kinetic study. For the kinetic investigation, 5-ATP-GO was added at the optimized dosage into separate Erlenmeyer flasks, each containing 50 mL of heavy metal solution prepared at the corresponding optimized pH and initial metal ion concentration. The mixtures were maintained at RT and subjected to sonication at 20–25 kHz and 60 W for predetermined time intervals of 5, 10, 30, 90, 150, and 300 minutes. The

Table 2 Experimental parameters and their levels

No	Coded	Parameter	Low level(-1)	High level(+1)
1	X_1	pH	4	10
2	X_2	Adsorbent dose (mg)	10	20
3	X_3	Initial metal ion concentrations (ppm)	20	50

Table 3 Equilibrium study models and the definition of their constants

Kinetic study	PFO	$q_t = q_e(1 - \exp(-K_1 t))$	K_1: PFO constant
			K_2: PSO constants
	PSO	$q_t = K_2 q_e^2 t/(1 + K_2 q_e t)$	q_e: Adsorption capacity at equilibrium
			q_t: Capacity of adsorption at time t
Isotherm study	Freundlich	$q_e = K_F C_e^{1/n}$	K_F Freundlich isotherm constants
	Sips	$q_e = q_M (K_s C_e)^n/(1 + (K_s C_e)^n)$	K_S: Sips isotherm constants
	Langmuir	$q_e = q_M K_L C_e/(1 + K_L C_e)$	K_L Langmuir isotherm constants
			n: Isotherm model exponent
			q_M: Maximum adsorption capacity
Modelling calculations	SSE	$\text{SSE} = \sum_{i=1}^{j}(q_{exp} - q_{cal})_i^2$	q_{exp}: ith values of the experimental adsorption capacity
			q_{cal}: ith values of the predicted adsorption capacity, respectively
			j: Number of observations

adsorption rate was tested by fitting the testing records within nonlinear mathematical equations; that is, pseudo-second-order (PSO) and pseudo-first-order (PFO) (Table 3).[40,41]

2.5.2 Isotherm study. For the isotherm experiments, the same optimized conditions were applied except for the variation in initial metal ion concentrations, which were set at 50, 75, 100, and 150 mg L^{-1}. The mixtures were sonicated for 2 h under identical conditions, and the equilibrium data were analyzed using nonlinear forms of Freundlich, Langmuir, and Sips isotherm models (Table 3).[40]

2.5.3 Modeling calculations. This section was carried out using the GRG (Generalized Reduced Gradient) non-longitudinal procedure of the Excel formulas calculation. The parameters were determined by minimizing the summation of squared error (SSE) function (Table 3).

2.6 The effect of interfering ions

The adsorption performance of 5-ATP-GO toward mercury, cadmium, and arsenic was evaluated to assess its selectivity in a multi-metal system. For this purpose, 60 mL mixed-metal solution containing 20 mg L^{-1} of each metal ion (Hg(II), Cd(II), and As(III); 1 : 1 : 1) was prepared, and the pH was adjusted to 8. The mixture was sonicated for 2 h (20–25 kHz, 60 W) at RT to ensure uniform dispersion of the adsorbent and promote effective interaction with the metal ions. After the adsorption process, the entire solution was centrifuged (6000 rpm, 10 min) and then filtered. The residual concentrations of the heavy metals were determined using GF-AAS. To ensure the reliability of the findings, all selectivity experiments were conducted in triplicate.

2.7 Recuperation study

The reusability of the 5-ATP-GO adsorbent was evaluated by conducting three adsorption–desorption cycles. Initially, 20 mg of 5-ATP-GO was added to 50 mL of a 50 mg L^{-1} heavy metal solution at the optimum pH (as determined by CCD) and RT. After adsorption, desorption was carried out by sonicating the used adsorbent with 30 mL of 1.0 M HCl for 3 minutes (20–25 kHz, 60 W). Subsequently, the material was thoroughly rinsed with distilled water until the pH exceeded 5, followed by drying. The concentration of residual heavy metals after each cycle was measured using GF-AAS. The elution conditions including 3 minutes of sonication and 1.0 M HCl were chosen in accordance

with the relevant literature,[19,20,42–44] which has shown these parameters to be effective for the regeneration of adsorbents with minimal degradation and efficient heavy metal desorption. All adsorption–desorption cycle experiments were performed in triplicate to ensure reproducibility and statistical reliability.

2.8 Model accuracy

The adsorption models were confirmed by the hybrid fractional error function (HYBRID), the determination coefficient (R^2), and the chi error (χ^2), which are defined as follows:[45]

$$R^2 = \left[\sum_{i=1}^{j}\left(q_{exp_i} - \overline{q_{exp}}\right)\left(q_{cal_i} - \overline{q_{cal}}\right)\right]^2 \Bigg/ \left[\sum_{i=1}^{j}\left(q_{exp_i} - \overline{q_{exp}}\right)^2\right.$$
$$\left.\times \sum_{i=1}^{j}\left(q_{cal_i} - \overline{q_{cal}}\right)^2\right]$$

(4)

$$\text{HYBRID} = \frac{100}{j - p}\left(\sum_{i=1}^{j}\left[\left(q_{exp} - q_{cal}\right)^2 \Big/ q_{exp}\right]_i\right) \quad (5)$$

$$\chi^2 = \sum_{i=1}^{j}\left[\left(q_{exp} - q_{cal}\right)^2 \Big/ q_{exp}\right] \quad (6)$$

where j is the numeral of experimental data points and p indicates the number of parameters in the fitted models. $\overline{q_{exp}}$ and $\overline{q_{cal}}$ are the average of q_{exp} and q_{cal}, respectively.[40,45]

3 Outcome and considering

3.1 Description of GO and 5-ATP-GO

The adsorbents were characterized by employing several techniques namely FTIR spectroscopy, TGA, XRD, EDX spectroscopy, FE-SEM, Raman spectroscopy, BET analysis, and ZP to compare the properties of the graphene ingredients and to further predict their behavior in the heavy metal adsorption process.

The infrared spectra of 5-ATP, GO, and 5-ATP-GO, which were recorded to investigate the successful modification of GO with 5-ATP, are presented in Fig. 2. The continuums of three materials show a broad band at ~3400 cm^{-1}, which is attributed to the OH stretching vibration of GO and the N–H stretching vibration of 5-ATP. Due to the overlap of O–H with
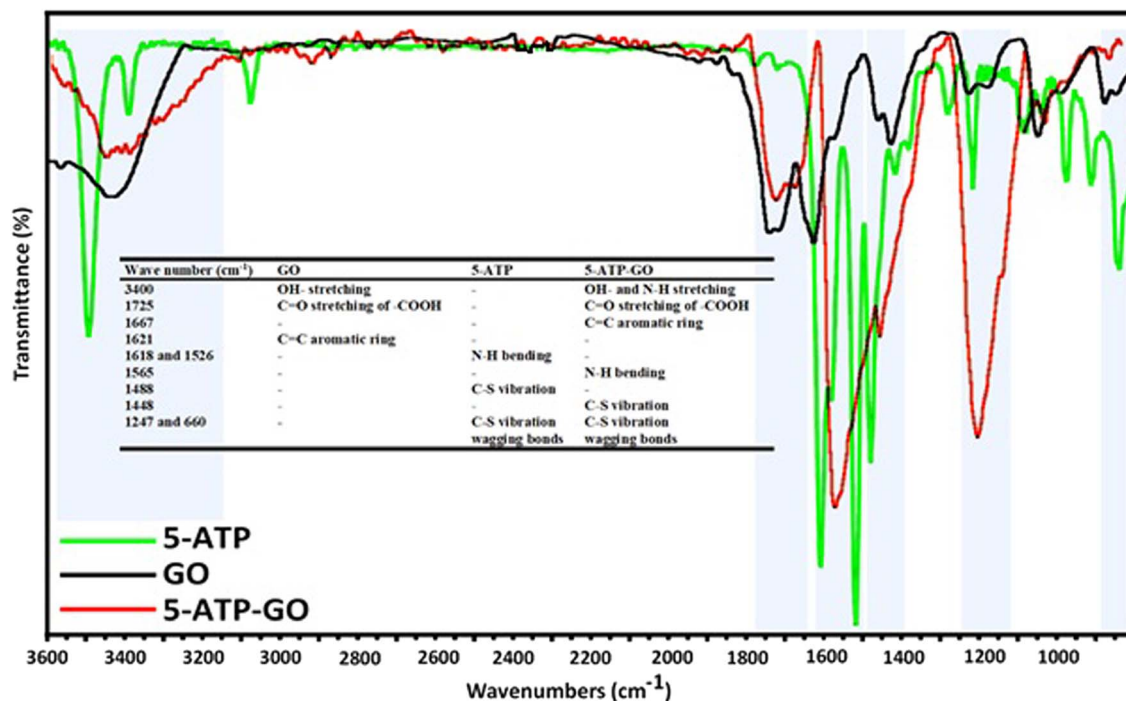
Fig. 2 FTIR spectra of GO and 5-ATP-GO composites.

the N–H band in 5-ATP-GO, this becomes a broad and intense signal.[15,17,18,46,47] In the region of 2300 to 2400 cm^{-1} in the FTIR spectrum, absorption peaks related to compounds such as carbon dioxide (CO_2) or isocyanate groups (–N=C=O) are usually observed. In the case of GO, this region can be attributed to the absorption of CO_2 from the environment, because GO has a high tendency to absorb environmental gases due to its porous structure and oxygen-containing groups.[48,52] In Fig. 2, an evident peak appears for GO and 5-ATP-GO at ∼1725 cm^{-1} that could be ascribed to conjugated C=O stretching of –COOH. It is also necessary to mention that the band on GO at 1621 cm^{-1} (C=C aromatic ring skeleton stretching vibration) was transferred to 1667 cm^{-1} in 5-ATP-GO, which corresponds to the vibration of N–H after the functionalization. Moreover, the two sharp peaks at 1618 and 1526 cm^{-1} for 5-ATP, which can

be ascribed to the N–H bending vibration have been merged into a broad peak at 1565 cm^{-1} for 5-ATP-GO (Fig. 2). The infrared band found at 1488 cm^{-1} might be allocated to C–S stretching of 5-ATP, and a similar but less pronounced peak (1448 cm^{-1}) was observed for 5-ATP-GO.[53] These peaks are present for 5-ATP and 5-ATP-GO, while the peak for GO is absent. Substantially, peaks at 660 cm^{-1} and 1247 cm^{-1} of 5-ATP that could be attributed to the C–S vibration and wagging bonds were also found after the functionalization process. The results of FTIR spectroscopy confirmed the successful attachment of functional groups in 5-amino-3(2-thienyl)pyrazole on graphene oxide and the partially maintained O-functional groups *via* substitution reaction.

Comparative thermogravimetric (TG) and derivative thermogravimetric (DTG) curves of GO and 5-ATP-GO, as presented
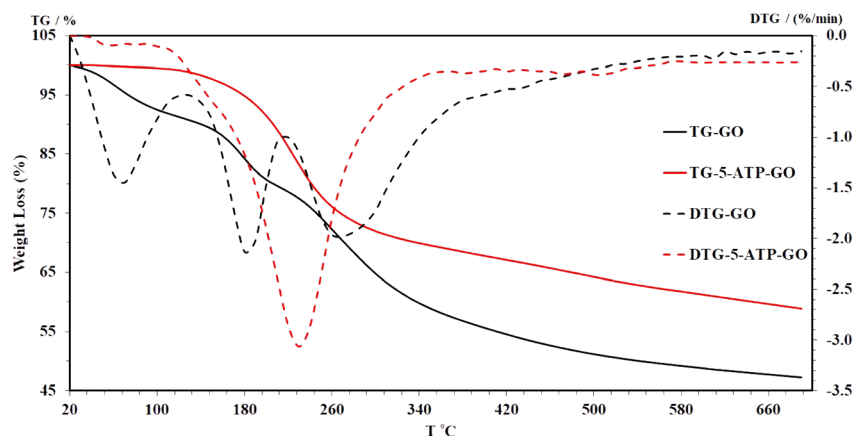

Fig. 3 Thermogravimetric and derivative thermogravimetric curves of GO and 5-ATP-GO.

in Fig. 3, were used to confirm the substitution reaction in 5-ATP-GO. Three distinct stages of mass losses were detected on GO, while only two were identified on 5-ATP-GO. The first weight loss, occurring below 120 °C, can be assigned to the evaporation of interstitial water and moisture, which represents about 8.75% for GO and 0.85% for 5-ATP-GO.[19] The second weight loss in GO (~11.5%) occurred at 210 °C (DTG minimum at ~180 °C), which can be related to the elimination of O-containing functional groups.[47] Afterward, the final mass loss of ~32.2% observed around 690 °C in the TG curve of the GO sample can be attributed to the pyrolysis of the carbon backbone.[55] Three peaks can be identified in the DTG curve of the GO, indicating the highest rates of weight loss (Fig. 3). In comparison with GO, 5-ATP-GO exhibited a sharp weight loss between 148 and 244 °C, which is attributed to the decomposition of functional groups formed *via* substitution of hydroxyl by amino groups. The comparison indicates that in the case of 5-ATP-GO, the starting temperature of loss of mass (148 °C) increased, while GO was decayed at a meaningfully lower temperature (36 °C). This means that 5-ATP-GO features a higher stability against temperature change (weight loss of ~39% totally) compared to GO (weight loss of ~53% totally),

representing a higher stability of functional groups including oxygen-bonded with 5-ATP moieties. Fig. 3 shows a main 5-ATP-GO peak from 120 to 360 °C (DTG at ~225 °C) that can be related to the decomposition of 5-ATP moieties. A relatively notable residual mass (~5.9%) was also observed in 5-ATP-GO from 410 to 620 °C, further supporting the successful incorporation of heteroatoms such as nitrogen and sulfur from 5-ATP.[18,56]

The XRD patterns of GO and 5-ATP-GO are shown in Fig. 4. The GO sample shows a sharp and intense peak at $2\theta = 11.04°$ (*d*-spacing = 8.01 Å), corresponding to the (001) reflection, which indicates a well-ordered layered structure of graphene oxide due to the presence of abundant oxygen-containing functional groups. This strong peak confirms the high degree of oxidation and interlayer spacing expansion in GO sheets.[49] After the functionalization of GO with 5-ATP, this peak (001) was not observed, demonstrating that some O-containing assemblies are compact in 5-ATP-GO, which could be endorsed to the starter of C–S- or C–N- groups on 5-ATP-GO after the substitution reaction. A sharp peak at $2\theta = 24.89°$ with a corresponding lower inner layer positioning of 3.57 Å exists in the XRD pattern of 5-ATP-GO, which is the (002) replication of the smaller amount oxidation of periodicity of loading in 5-ATP-GO. These results support that carboxyl groups on GO reacted with the amine moiety of 5-ATP, leading to the formation of a more disordered but chemically functionalized structure. Similar observations have been reported in previous works.[19,58,59]

EDX spectra indicated a clear difference in the elemental composition of GO and 5-ATP-GO. As shown in Fig. 5, only oxygen (O) and carbon (C) peaks can be seen in the EDX spectra of the GO sample, confirming that its structure primarily consists of oxygenated carbon frameworks. In contrast, the 5-ATP-GO spectrum displays additional peaks for sulfur (S) and nitrogen (N), which are absent in pristine GO. These peaks provide strong evidence of successful functionalization with 5-ATP, which contains both sulfur and nitrogen atoms in its structure. A significant reduction in the O/C atomic ratio from 1.1 in GO to 0.27 in 5-ATP-GO was observed, indicating that
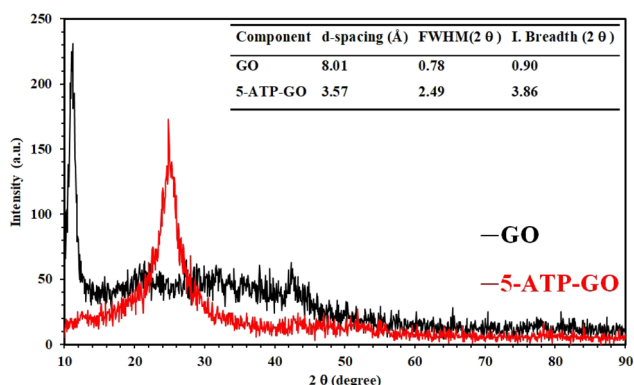

Component	d-spacing (Å)	FWHM (2 θ)	I. Breadth (2 θ)
GO	8.01	0.78	0.90
5-ATP-GO	3.57	2.49	3.86

Fig. 4 XRD diffractograms of GO and 5-ATP-GO.

Element	W%	A%
C	47.36	54.51
O	52.64	45.49

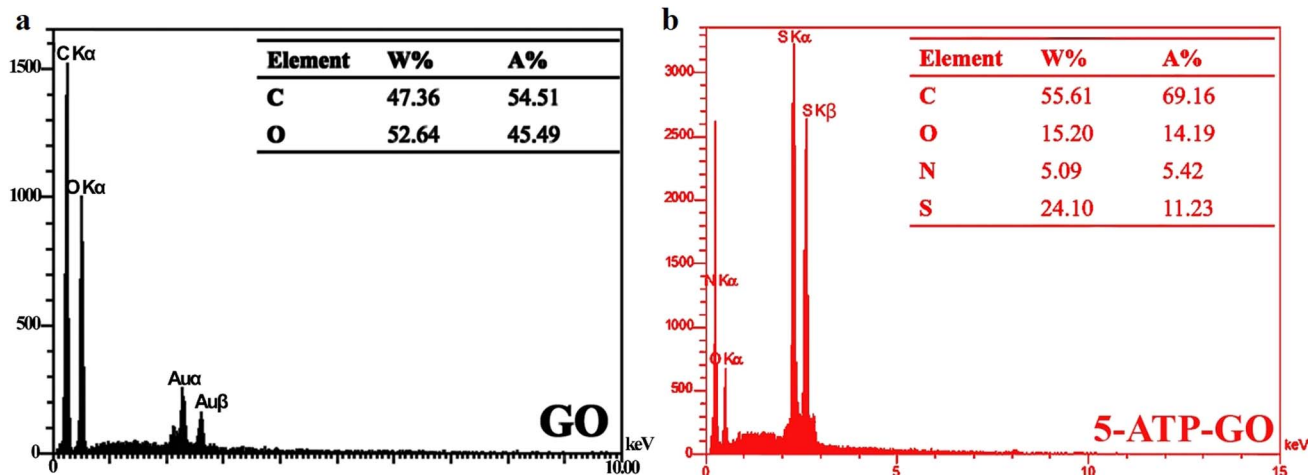| Element	W%	A%
C	55.61	69.16
O	15.20	14.19
N	5.09	5.42
S	24.10	11.23

Fig. 5 EDX spectrum of (a) GO and (b) 5-ATP-GO.

a substantial portion of oxygen-containing groups was substituted during the modification process. This transformation highlights the effective attachment of 5-ATP through covalent bonding, particularly involving the reaction of amine or thiophene groups with the oxygen functionalities on GO. This chemical modification is expected to enhance the adsorptive capacity of the material by: (1) introducing strong donor atoms (N and S) capable of chelating heavy metal ions, (2) reducing surface polarity, and (3) expanding the π-conjugated domain, thus improving the electron-donating capability.

GO and 5-ATP-GO were examined in terms of particle morphology using FE-SEM. As shown in Fig. 6, GO exhibits aggregated, crumpled, and irregular layers, leading to limited surface accessibility. The surface is wavy and wrinkled due to the strong interactions among hydrophilic oxygen-containing groups, which also promote stacking of the GO sheets.[52] After functionalization, 5-ATP-GO demonstrates flatter, more evenly distributed sheet structures with noticeably smoother surfaces. This change in morphology is attributed to the grafting of amino-thienyl ligands on both the edges and basal planes of the GO, which reduces the stacking tendency and creates more accessible active sites. Moreover, slight overlaps between several layers of 5-ATP-GO sheets are evident in the SEM image, indicating partial re-aggregation but with increased interlayer spacing. These structural modifications confirm the successful surface functionalization and imply an improved morphology for adsorption applications. The more dispersed and open-layered structure of 5-ATP-GO facilitates better interaction with heavy metal ions and enhances its adsorption efficiency.

To further analyze the structural changes induced by functionalization, the Raman spectra of GO and 5-ATP-GO are presented in Fig. 7. In the spectrum of GO, two major peaks are observed: The D band at approximately 1355 cm^{-1}, which corresponds to disordered structures and defects in the sp^2 carbon framework, and the G band at around 1605 cm^{-1}, attributed to the in-plane vibration of sp^2 carbon atoms in graphitic domains. Upon functionalization with 5-ATP, both D and G bands exhibit shifts: the D band moves to ~1345 cm^{-1} and the G band to ~1540 cm^{-1}, reflecting changes in the vibrational structure due to chemical modification.[53] Additionally, the I_D/I_G intensity ratio (the intensity of the D-band to the
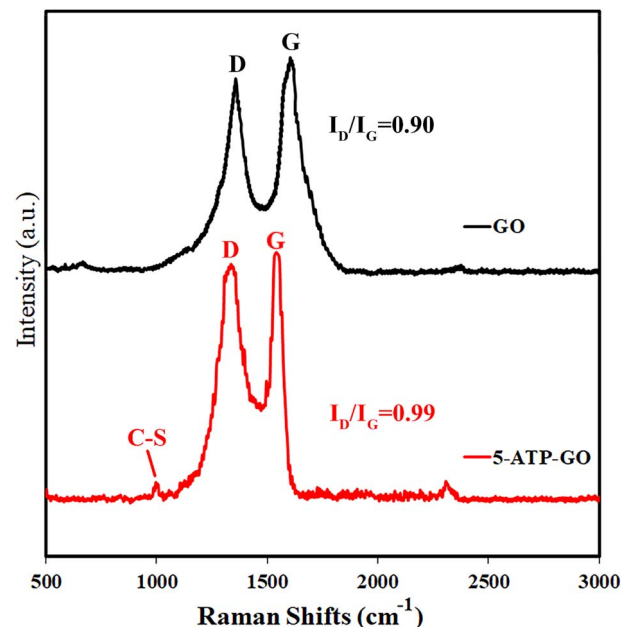

Fig. 7 Comparison of the Raman spectra for GO and 5-ATP-GO.

G-band) increases from 0.90 (GO) to 0.99 (5-ATP-GO). According to defect evolution theory, this increase indicates a decrease in structural disorder and an increase in the average size of sp^2 domains, as GO lies in the high-defect region of the I_D/I_G bell-shaped distribution. Furthermore, a distinct peak at ~1005 cm^{-1}, attributed to the C–S stretching vibrations, appears in 5-ATP-GO, providing direct evidence for the presence of sulfur-containing functional groups.[54] These observations collectively confirm that 5-ATP was successfully grafted onto the GO surface, introducing new functionalities and modifying the carbon framework, consistent with the findings from similar studies.[53]

The specific surface area and pore size are the essential parameters touching the adsorption performance of nanomaterials. Generally, the adsorbents with a larger specific surface space can achieve better adsorption performance. As shown in Fig. 8 and detailed in Table 4, BET analysis was performed to evaluate the surface characteristics of GO and 5-ATP-
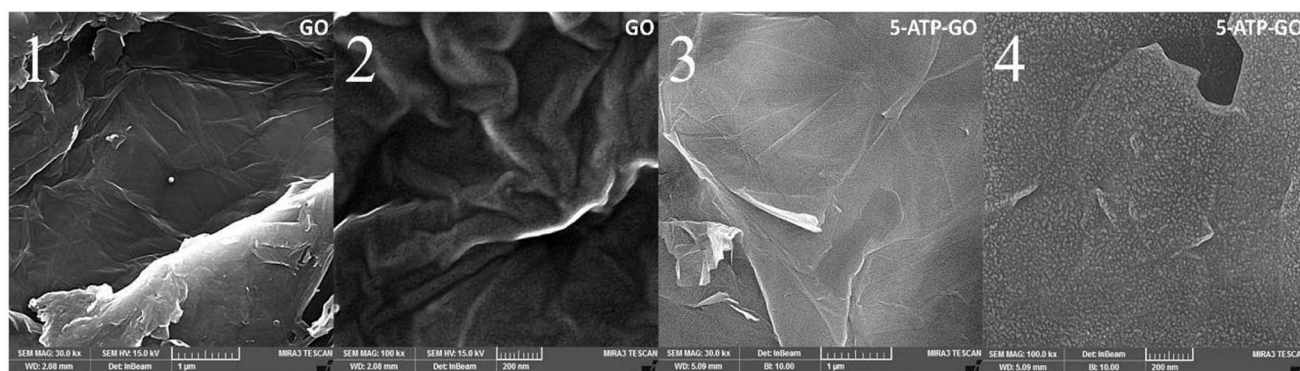

Fig. 6 SEM images of GO and 5-ATP-GO captured at two different resolutions: 1 μm and 200 nm.

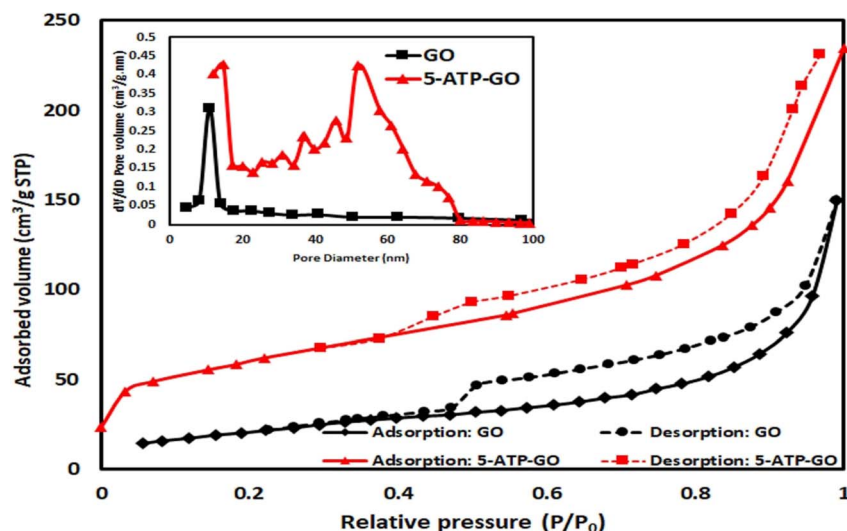© 2025 The Author(s). Published by the Royal Society of Chemistry

Fig. 8 BET analysis and pore diameter distribution of GO and 5-ATP-GO.

GO. The N_2 adsorption–desorption isotherms of 5-ATP-GO referred to the type II hysteresis loop (according to the IUPAC classification), showing a combination of monolayer and multilayer physisorption without significant pore restrictions. This proposes that the adsorption of nitrogen can be indorsed to van der Waals forces on the surface of the composite. BET analysis reveals that the specific surface area of GO was 69.44 $m^2\ g^{-1}$, and it was increased to 215.53 by functionalization with 5-ATP, demonstrating enhanced accessible surface sites due to exfoliation and surface modification. A similar increasing trend was observed in total pore volume and average pore size, supporting the formation of a more porous and accessible structure. These changes confirm that the grafting of 5-ATP introduced new structural features, contributing to a greater adsorption capacity, which is essential for heavy metal removal applications.

The zeta potential (ZP) analysis was performed to evaluate the surface charge behavior of GO and 5-ATP-GO across a pH range of 2 to 10 (Fig. 9). All measurements were conducted in triplicate, and the average values were reported to ensure reproducibility. Both materials exhibited negative ZP values, indicating the presence of negatively charged functional groups on their surfaces. The ZPs of GO ranged from −15 to −57 mV, whereas 5-ATP-GO showed more negative values between −23 and −72 mV. Since colloidal suspensions with a ZP beyond ±30 mV are generally considered stable, the more negative ZPs of 5-ATP-GO confirm its enhanced dispersion stability, which can be attributed to increased hydrophilicity and electrostatic repulsion due to functionalization. Moreover, the trend of
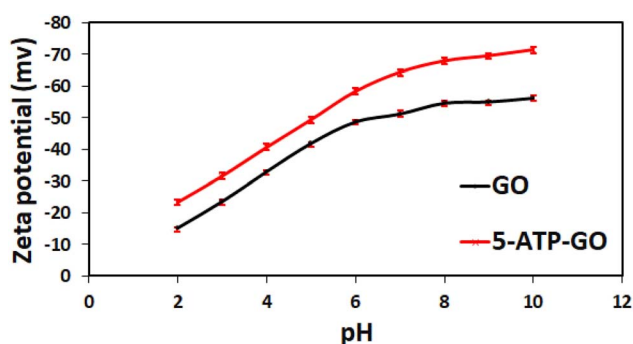

Fig. 9 Zeta-potentials of GO and 5-ATP-GO at different pH values.

increasingly negative ZPs with the increase in pH suggests that the deprotonation of surface functional groups enhances electrostatic interactions, particularly with positively charged metal ions. This behavior confirms that the 5-ATP-GO composite remains stable and effective across a wide pH range and supports its potential in adsorption applications.

3.2 Adsorption process modeling by CCD

To optimize the process conditions for Hg(II), Cd(II), and As(III) adsorption onto 5-ATP-GO and GO surfaces, the CCD technique was employed, and the results are recorded in Table 1. Experimental data were analyzed using ANOVA, with the results provided in Tables 5 and 6. This analysis makes it possible to identify the effects and interactions of variables on adsorption efficiency, ensuring the statistical validity of the findings. Predicted values were compared with experimental data, and statistical indicators such as p-value and F-test were calculated to assess the significance of the variables.

Based on the CCD results in Tables 5 and 6, polynomial regression models were developed to describe the interactions among the three variables, and the final equations obtained are as follows:

Table 4 BET results of Go and 5-ATP-GO

Material	GO	5-ATP-GO
Pore volume ($cm^3\ g^{-1}$)	0.0204	0.3483
BET surface ($m^2\ g^{-1}$)	69.44	215.53
Pore size (nm)	2.46	6.465

Table 5 Results of ANOVA for the response surface method using quadratic models for the removal of Cd(II), As(III), and Hg(II) by GO[a]

Source	Sum of squares			df	Mean square			F value			p-value prob > F		
	Cd^{+2}	Hg^{+2}	As^{+3}		Cd^{+2}	Hg^{+2}	As^{+3}	Cd^{+2}	Hg^{+2}	As^{+3}	Cd^{+2}	Hg^{+2}	As^{+3}
Model	0.069	3.634	4.191	9	0.008	0.404	0.466	643.253	612.838	321.097	<0.0001	<0.0001	<0.0001
X_1	0.023	0.843	0.728	1	0.023	0.843	0.728	1885.852	1279.394	501.614	<0.0001	<0.0001	<0.0001
X_2	0.003	0.199	0.399	1	0.003	0.199	0.399	231.992	301.625	274.798	<0.0001	<0.0001	<0.0001
X_3	0.015	0.913	0.768	1	0.015	0.913	0.768	1293.558	1385.660	529.640	<0.0001	<0.0001	<0.0001
X_1X_2	0.000	0.005	0.008	1	0.000	0.005	0.008	0.739	6.993	5.275	0.410	0.0245	0.0445
X_1X_3	0.000	0.005	0.025	1	0.000	0.005	0.025	33.734	8.137	17.355	0.0002	0.0172	0.0019
X_2X_3	0.000	0.008	0.006	1	0.000	0.008	0.006	3.763	12.668	4.241	0.081	0.0052	0.0665
X_1^2	0.026	1.503	2.212	1	0.026	1.503	2.212	2190.580	2280.745	1524.992	<0.0001	<0.0001	<0.0001
X_2^2	0.000	0.000	0.002	1	0.000	0.000	0.002	5.808	0.138	1.376	0.0367	0.7180	0.2679
X_3^2	0.003	0.234	0.103	1	0.003	0.234	0.103	258.613	355.817	71.108	<0.0001	<0.0001	<0.0001
Residual	0.000	0.007	0.015	10	0.000	0.001	0.001						
Lack of fit	0.000	0.005	0.011	5	0.000	0.001	0.002	4.916	5.030	2.701	0.0527	0.0504	0.150
Pure error	0.000	0.001	0.004	5	0.000	0.000	0.001						
R^2	0.998	0.998	0.997										
Adj-R^2	0.997	0.997	0.993										
Pred-R^2	0.989	0.987	0.978										
SD	0.004	0.026	0.038										
C.V%	2.29	1.67	3.35										

[a] X_1: pH, X_2: adsorbent doses (mg), X_3: original metal ion concentration (mg L^{-1}).

Table 6 Results of ANOVA for the response surface method using quadratic models for the removal of Cd(II), As(III), and Hg(II) by 5-ATP-GO[a]

Source	Sum of squares			df	Mean square			F value			p-value prob > F		
	Cd^{+2}	Hg^{+2}	As^{+3}		Cd^{+2}	Hg^{+2}	As^{+3}	Cd^{+2}	Hg^{+2}	As^{+3}	Cd^{+2}	Hg^{+2}	As^{+3}
Model	0.062	0.054	1.976	9	0.007	0.006	0.220	1423.914	1681.244	319.767	<0.0001	<0.0001	<0.0001
X_1	0.022	0.017	0.009	1	0.022	0.017	0.009	4568.727	4684.478	12.560	<0.0001	<0.0001	0.005
X_2	0.004	0.003	0.202	1	0.004	0.003	0.202	877.031	913.138	294.398	<0.0001	<0.0001	<0.0001
X_3	0.014	0.013	0.535	1	0.014	0.013	0.535	2790.718	3590.517	779.674	<0.0001	<0.0001	<0.0001
X_1X_2	0.000	0.000	0.001	1	0.000	0.000	0.001	3.944	6.311	1.943	0.075	0.031	0.194
X_1X_3	0.000	0.001	0.000	1	0.000	0.001	0.000	61.554	148.653	0.680	<0.0001	<0.0001	0.429
X_2X_3	0.000	0.000	0.007	1	0.000	0.000	0.007	5.880	0.584	10.172	0.036	0.462	0.010
X_1^2	0.020	0.019	0.926	1	0.020	0.019	0.926	4185.887	5360.709	1349.126	0.000	<0.0001	<0.0001
X_2^2	0.000	0.000	0.016	1	0.000	0.000	0.016	0.761	16.433	22.921	0.403	0.002	0.001
X_3^2	0.002	0.002	0.318	1	0.002	0.002	0.318	474.329	538.153	463.463	<0.0001	<0.0001	<0.0001
Residual	0.000	0.000	0.007	10	0.000	0.000	0.001						
Lack of fit	0.000	0.000	0.006	5	0.000	0.000	0.001	4.520	4.638	4.082	0.0620	0.059	0.074
Pure error	0.000	0.000	0.001	5	0.000	0.000	0.000						
R^2	0.999	0.999	0.997										
Adj-R^2	0.999	0.999	0.993										
Pred-R^2	0.995	0.996	0.978										
SD	0.002	0.002	0.026										
C.V%	1.63	1.38	1.79										

[a] X_1: pH, X_2: adsorbent dose (mg), X_3: initial metal ion concentrations (mg L^{-1}).

$$y_{Hg(II)}^{GO} = \log(q - 6) = -1.57 + 0.64 \times X_1 - 0.03 \times X_2 + 0.05 \times X_3 - 1.6 \times 10^{-3} \times X_1X_2 - 5.7 \times 10^{-4} \times X_1X_3 + 4.3 \times 10^{-4} \times X_2X_3 - 0.04 \times X_1^2 - 5.75 \times 10^{-4} \times X_3^2 \quad (7)$$

$$y_{Cd(II)}^{GO} = q^{-0.5} = 0.61 - 0.09 \times X_1 + 8.50 \times 10^{-4} \times X_2 - 7.51 \times 10^{-3} \times X_3 + 1.58 \times 10^{-4} \times X_1X_3 + 4.81 \times 10^{-3} \times X_1^2 + 8.7 \times 10^{-5} \times X_2^2 + 6.61 \times 10^{-5} \times X_3^2 \quad (8)$$

$$y_{As(III)}^{GO} = \log(q - 4) = -1.74 + 0.71 \times X_1 - 0.05 \times X_2 + 0.05 \times X_3 + 2.06 \times 10^{-3} \times X_1X_2 - 1.25 \times 10^{-3} \times X_1X_3 - 0.04 \times X_1^2 - 3.81 \times 10^{-4} \times X_3^2 \quad (9)$$

$$y_{Hg(II)}^{5\text{-}ATP\text{-}GO} = (q - 2)^{-0.5} = 0.49 - 0.07 \times X_1 + 6.00 \times 10^{-3} \times X_2 - 7.03 \times 10^{-3} \times X_3 - 1.11 \times 10^{-4} \times X_1X_2 + 1.80 \times 10^{-4} \times X_1X_3 + 4.09 \times 10^{-3} \times X_1^2 - 7.96 \times 10^{-5} \times X_2^2 + 5.18 \times 10^{-5} \times X_3^2 \quad (10)$$

$$y_{Cd(II)}^{5\text{-}ATP\text{-}GO} = (q - 2)^{-0.5} = 0.50 - 0.08 \times X_1 + 5.73 \times 10^{-3} \times X_2 - 6.67 \times 10^{-3} \times X_3 + 1.36 \times 10^{-4} \times X_1X_3 - 2.52 \times 10^{-3} \times X_2X_3 + 4.23 \times 10^{-3} \times X_1^2 + 5.70 \times 10^{-5} \times X_3^2 \quad (11)$$

Table 7 Optimum conditions for adsorption processes and model validation

Parameter	GO			5-ATP-GO		
	Hg(II)	Cd(II)	As(III)	Hg(II)	Cd(II)	As(III)
pH	8.03	8.67	7.72	7.89	8.20	7.25
Adsorbent dose (mg)	10.15	11.07	10.20	10.22	10.21	10.00
Initial metal ion conc. (ppm)	47.96	49.91	47.49	49.51	47.71	43.45
Predicted q (mg g^{-1})	134.65	168.88	61.39	242.58	275.47	88.09
Model desirability	1	1	1	1	1	0.77

$$y_{As(III)}^{5\text{-ATP-GO}} = \log(q-5) = -0.21 + 0.41 \times X_1 - 0.07 \times X_2 + 0.05 \times X_3 + 3.94 \times 10^{-4} \times X_2 X_3 - 0.03 \times X_1^2 + 1.31 \times 10^{-3} \times X_2^2 - 6.70 \times 10^{-4} \times X_3^2 \quad (12)$$

where X_3, X_2, and X_1 represent the preliminary metal ion amount, adsorbent dose, and pH, respectively.

Table 8 Optimal conditions for the validation of the kinetic and isotherm models

Adsorbent	Metal ion	pH	Adsorbent dosage (mg)	Initial ion conc. (ppm)
GO	Cd(II)	8.7	10	50
	Hg(II)	8.0		
	As(III)	7.7		
5-ATP-GO	Cd(II)	8.2	10	50
	Hg(II)	7.9		
	As(III)	7.3		

To examine the significance of the quadratic equation, the F-test was used at a confidence level of 95%.[19] As listed in Tables 5 and 6, with a p-value < 0.05, the linear parameters (the values of adsorbent, primary metal ion, and pH) and the quadratic terms of pH and initial metal ions concentrations are important for the 2 adsorbents. Furthermore, with adjusted R^2 > 0.99, the model is recommendable for predicting the actual adsorption process performance. The estimated R^2 value was almost similar to the adjusted R^2 value (Tables 5 and 6), and the coefficient of variation (CV = standard deviation/mean) is below 10%. Moreover, the accuracy of the model was supported by the standard deviations (SD < 0.038), indicating the good exactitude of the proposed routine.

To obtain the optimal situations to maximize responses, the prediction model was designed. Table 7 lists the optimum values for three variables based on the model. In comparison with unmodified GO, 5-ATP-GO demonstrates a higher q as to metal ions, particularly cadmium ions. Therefore, the metal
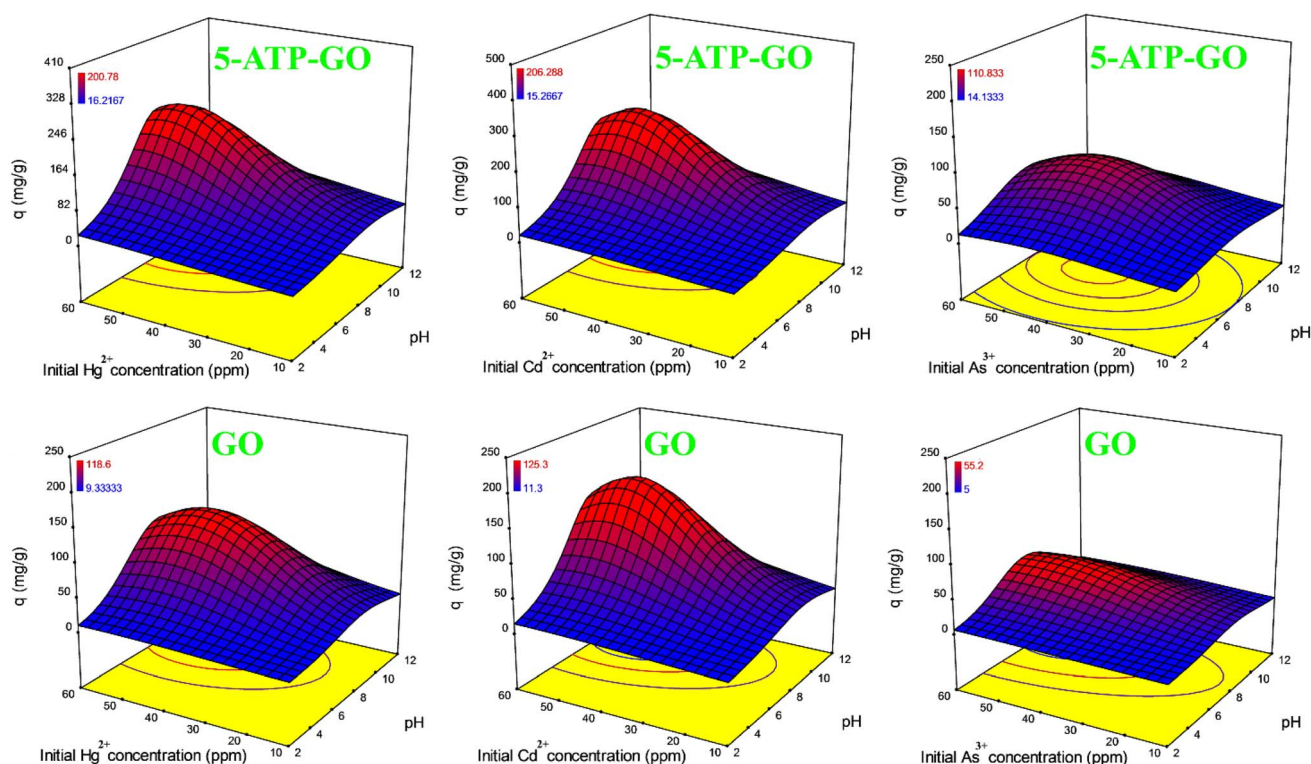

Fig. 10 3D schemes showing the effects of initial ion concentration and pH against the capacity of adsorption at a constant dose of adsorbent of 10 mg.
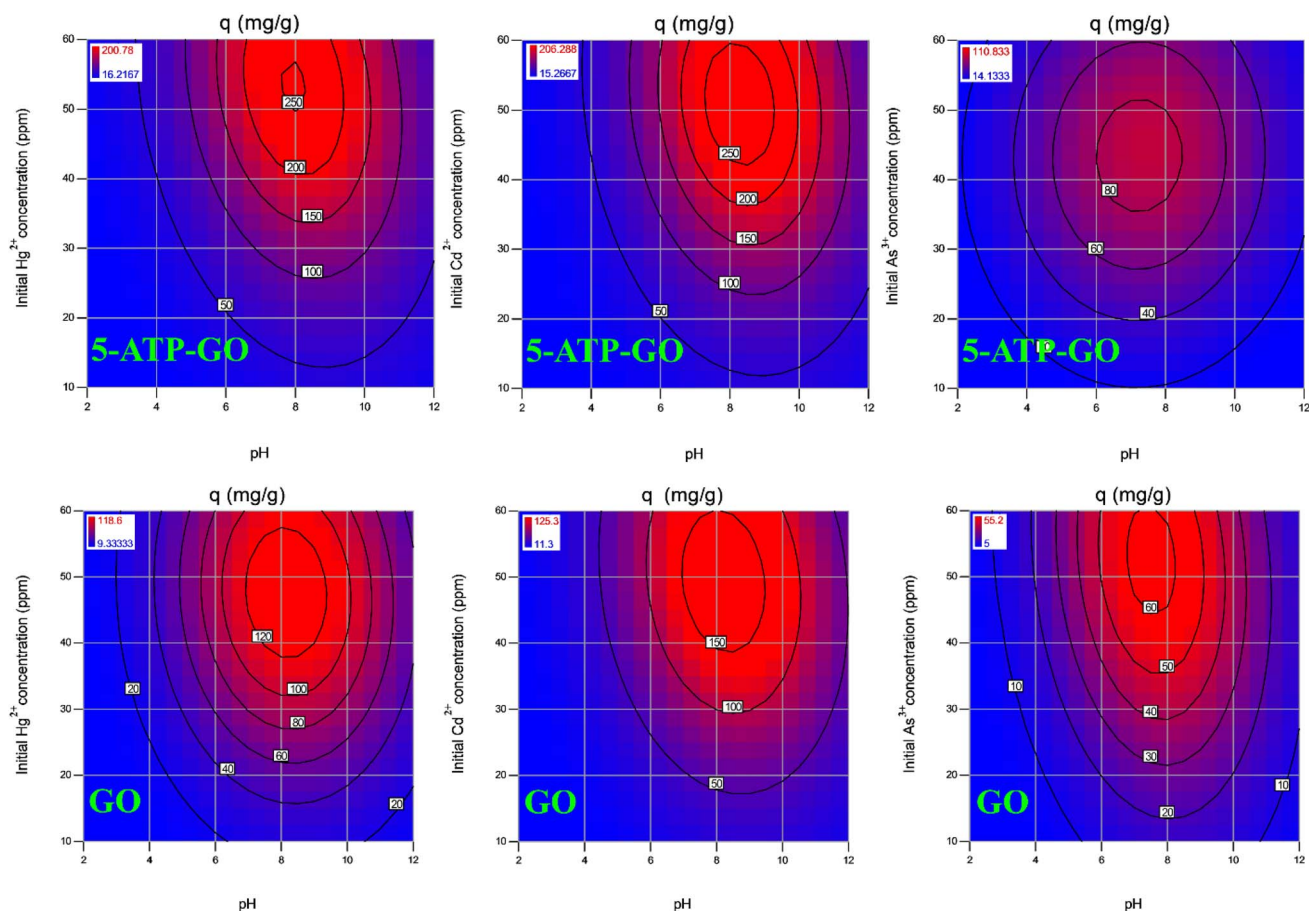
Fig. 11 2D drawings displaying pH and initial ion concentrations *versus* adsorption capacity at a constant adsorbent dose of 10 mg.
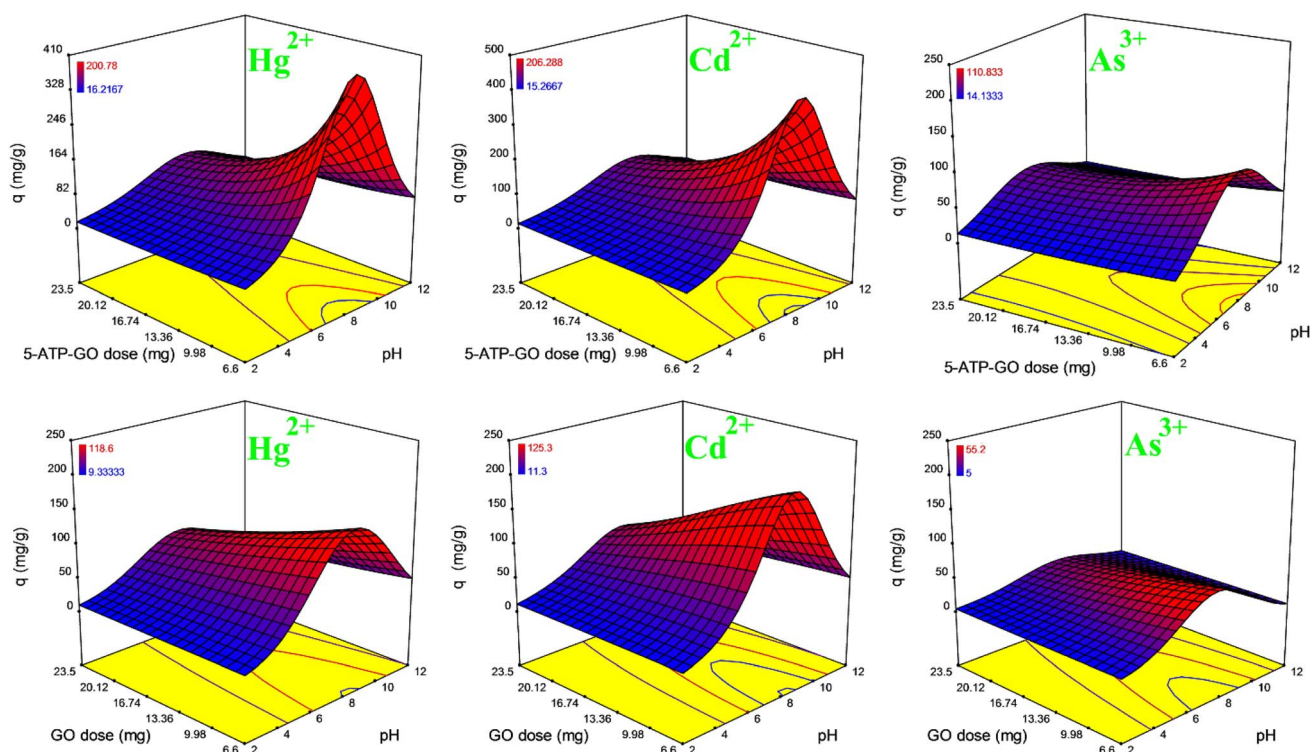

Fig. 12 The 3D plots presenting adsorbent dose and pH compared to the adsorption capacity at a constant initial ion concentrations of 50 ppm.

ions can bind to –COO-, –O-, –S-, and –N- on the surfaces of 5-ATP-GO to arrange complex compounds. Moreover, because of the distribution of Cd(ɪɪ) in a broader range of pH (<8.5) than that of other metal ions (Hg(ɪɪ) pH < 3 and As(ɪɪɪ) pH < 7.5), the capacity of Cd ion adsorption is more.[55–57] In expressions of kinetic parameters and isothermal models, experimental errors can be minimized by applying the optimum conditions listed in Table 8.

3.3 Response surface plotting

Assuming a significant interaction in the CCD, Fig. 10–13 illustrate the 2D and 3D response surface plots of the adsorption process. The graphs show the interaction of adsorbent doses, initial metal ion concentrations, and pH to the capacity of adsorption of sorbents, while the rest of the parameters remain unchanged with the optimum levels. The curvatures in the plots are examined based on the effects of the variables and their interaction.

3.3.1 Effect of initial metal ion concentrations and pH on q. The process of adsorption is greatly affected by the pH of solutions. This is because the interaction of cations with surface-active groups strongly depends on the surface charge of

the adsorbent, which is determined by the presence of OH⁻ and H⁺ ions in solutions.

Fig. 10 and 11 illustrate the 2D and 3D interactive impacts of pH and initial metal ion contents on the adsorption capacity (q) of As(ɪɪɪ), Hg(ɪɪ), and Cd(ɪɪ). This figure discloses that at lower pH values, q reduces due to the competition between hydronium ions and metal ions for available active sites. At higher pH, both GO and 5-ATP-GO adsorbents demonstrate higher q, although the q value of 5-ATP-GO is higher because of its highly active surface functional groups. The adsorbent surface charge gets negative with the increase in pH, which facilitates electrostatic interactions between the metal cations and the sorbent, which is consistent with the ZP investigation. However, at excessively high pH values, increased electrostatic repulsion may hinder adsorption. According to Fig. 10, by further increasing pH from 8, q of Cd(ɪɪ) decreases significantly, which is mainly attributed to the Cd hydrolysis; Cd(OH)⁺ species start to form at pH = 8.4 to 12.[58] The q value of Hg ions reduces at pH 8.4 to 12 because of the production of $Hg(OH)_3^-$ and $Hg(OH)_4^-$, and these complexes cannot be retained on the GO surface because of dissolving in liquid.[59] In the case of As(ɪɪɪ) adsorption, the trend is similar to the previous ions. This is because at higher pH (8–12), As ions existed in the anionic form ($H_2AsO_3^-$ and $HAsO_3^{-2}$). Moreover, in acidic
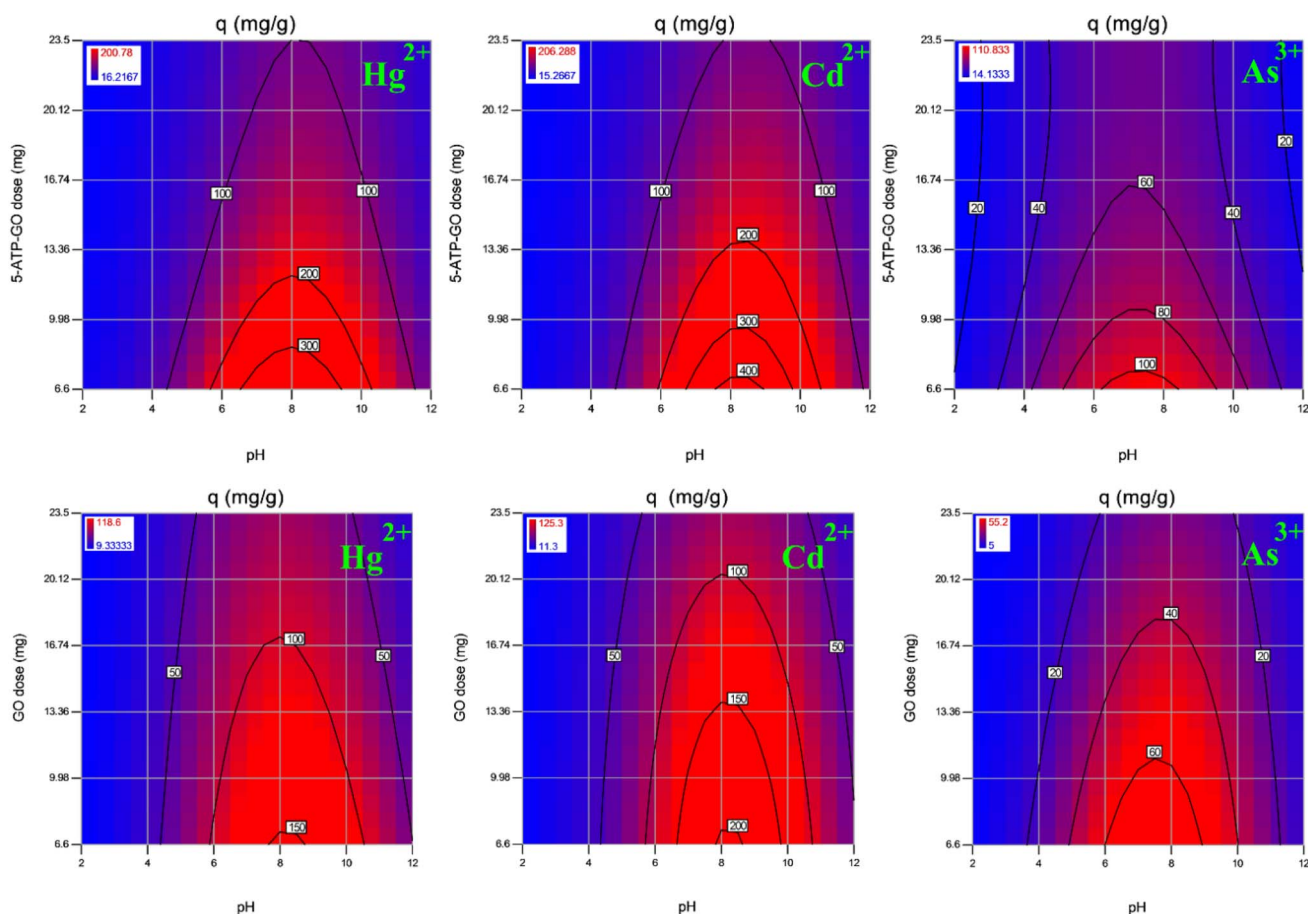

Fig. 13 3D schemes revealing variations in pH and adsorbent doses compared to the adsorption capacity at a constant initial ion concentrations of 50 ppm.

solutions (pH = 4–7), the solubility of As ions gets reduced, explaining the low q value of As ions at acidic pH.[60,61]

Furthermore, as shown in Fig. 11, by increasing the concentration of the initial metal ion from 10 to 60 ppm, the q value gradually increases and reaches a higher value at the persistent adsorbent dose (10 mg). It agrees with eqn (1), in which q is proportionate to the initial metal ion concentrations.

3.3.2 Effect of adsorbent dose and pH on q. Fig. 12 and 13 depict the interaction effects of pH and the adsorbent dose on the q value of As(III), Hg(II), and Cd(II) on 5-ATP-GO and GO. The effect of pH on the adsorption process varies depending on the type of surface functional groups. In the acidic regions, due to competition between hydronium ions and heavy metal ions for unpaired active sites, q is low. It was observed that by increasing the pH, q increased smoothly. As the pH increases, the complexes that form between metal ions and the adsorbent surface are increasingly stable due to the increasing negative charge of the surface, resulting in higher metal ion adsorption. The adsorption capacity decreases with further growth in pH which can be the reason for the precipitation of $Cd(OH)_2$, $Hg(OH)_2$, and the electrostatic repulsion of $HAsO_2$.[60]

Further, Fig. 12 and 13 reveal that by decreasing the amount of adsorbent from 23.5 to 6.6 mg, the adsorption capacity increased gradually and reached the maximum rate. For 5-ATP-GO, a steeper growth in the rate of adsorption was seen, which is compatible with eqn (1), in which the adsorption capacity drops as the adsorbent dose grows.

3.4 Adsorption equilibrium

3.4.1 Adsorption kinetics. Fig. 14a illustrates the adsorption kinetics of heavy metals (Hg(II), Cd(II), and As(III)) onto GO and 5-ATP-GO. The steep upward pattern of heavy metal uptake indicates an extremely rapid initial metal adsorption rate. About 80% Hg(II), 86% Cd(II), and 75% As(III) were removed by 5-ATP-GO (10 mg) within 30 minutes, and Hg(II), Cd(II), and As(III) uptake reached ~89%, ~99%, and ~86% at equilibrium for 5-ATP-GO adsorbents, respectively, while nearly 70%, 88%, and 36% of Hg(II), Cd(II), and As(III) were removed at equilibrium when GO adsorbent was used. From the adsorption kinetics aspect, the efficiency attained by 5-ATP-GO (30 min) is distinguished in comparison to other adsorbents prepared in our previous studies, 3-aminopyrazole-GO (60 min)[19] and 3-amino-5-phenylpyrazole-GO (60 min)[20] to achieve the adsorption equilibrium. Furthermore, concerning polyethyleneimine modified with the GO hydrogel composite prepared by Arshad et al.,[62] approximately 100 minutes (compared to 30 minutes for 5-ATP-GO) was needed to attain the adsorption equilibrium when an approximately higher sorbent dosage was used in their studies.

To gain additional insights into the mechanism of Hg(II), Cd(II), and As(III) adsorption onto 5-ATP-GO, the kinetic data were fitted to the nonlinear form of PFO and PSO models, as seen in Fig. 15. The fitting analysis results revealed that the PSO model provided the best fit with maximum R^2 and lower values of SSE, HYBRID, and $\chi2$ compared to the PFO model (Table 9).
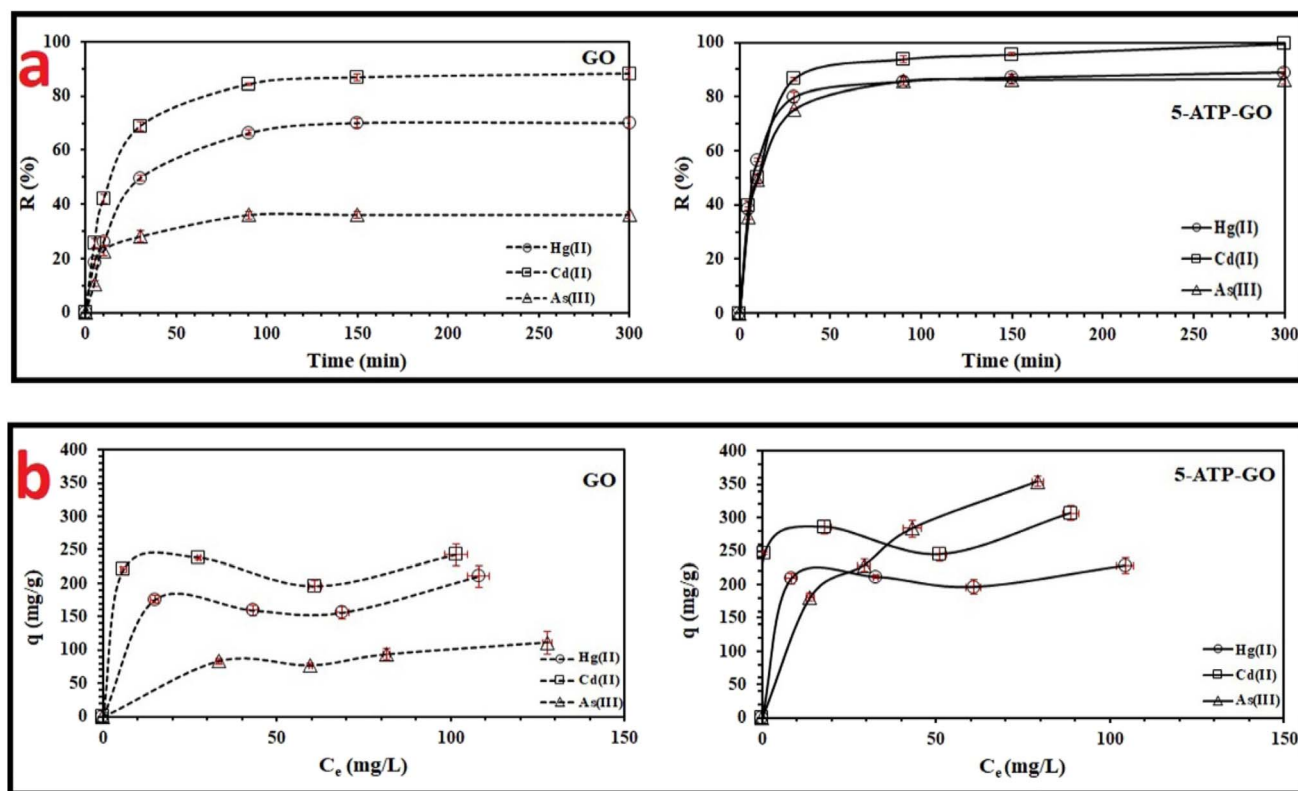

Fig. 14 (a) Variations in the adsorption efficiency with time and (b) adsorption capacity *versus* initial metal ion concentration effect investigation on Hg(II), Cd(II), and As(III) adsorption by 5-ATP-GO and GO.
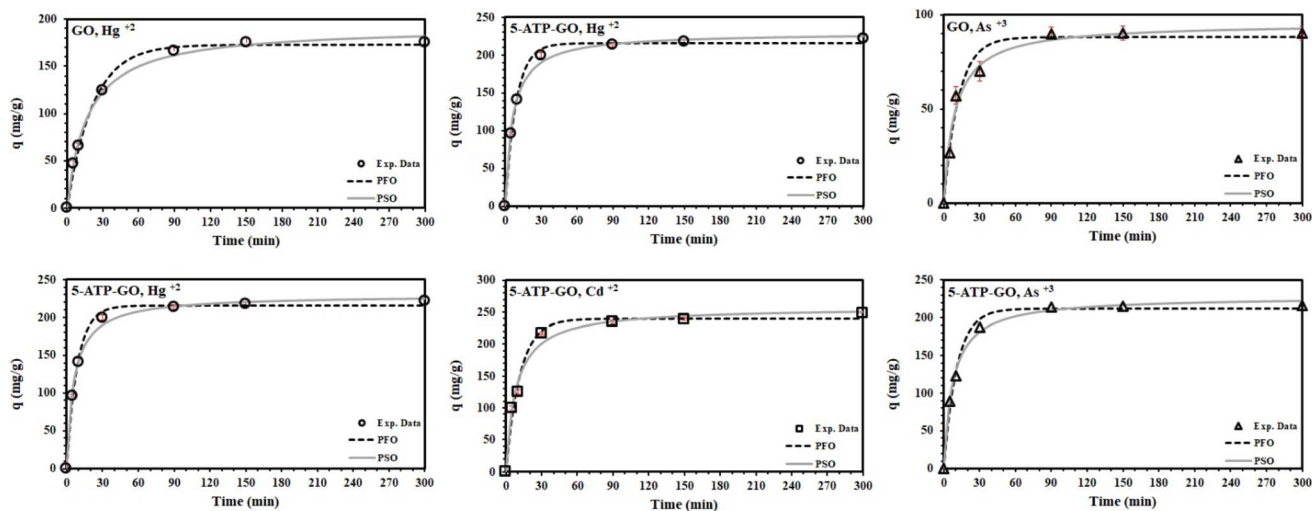
Paper

Fig. 15 Representation of the pseudo-second-order (PSO) and pseudo-first-order(PFO) kinetic relations for 5-ATP-GO and GO in nonlinear regression analysis by comparison with experimental data, for Hg(II), Cd(II), and As(III) sorption at 25 °C under optimum conditions.

Table 9 Nonlinear adsorption kinetic models and their parameters for the adsorption of Hg(II), Cd(II), and As(III) on GO and 5-ATP-GO

| Model	Parameter	GO			5-ATP-GO		
		Hg(II)	Cd(II)	As(III)	Hg(II)	Cd(II)	As(III)
Pseudo-first order	K_1	0.047	0.063	0.081	0.109	0.084	0.091
	q_e	172.684	214.747	88.214	215.551	239.364	212.309
	R^2	0.985	0.999	0.987	0.998	0.995	0.992
	SSE	184.068	213.056	196.289	150.404	535.456	280.597
	HYBRID	59.257	33.105	62.949	18.197	73.476	45.764
	χ^2	2.963	1.655	3.147	0.910	4.409	2.288
Pseudo-second order	K_2	3.8×10^{-4}	3.5×10^{-4}	0.001	6.93×10^{-4}	4.57×10^{-4}	0.001
	q_e	191.927	234.759	95.576	229.516	257.297	227.477
	R^2	0.994	0.999	0.991	0.998	0.995	1.000
	SSE	113.860	84.434	130.351	139.334	479.486	134.468
	HYBRID	22.680	12.358	61.273	16.647	48.667	14.997
	χ^2	1.134	0.618	3.064	0.832	2.920	0.750

PSO kinetic model reveals that the heavy metal adsorption contains a chemisorption process along with considering the available adsorption sites for the process of exchange at the solid–solution interface. This proposes that the rate-controlling step for heavy metal adsorption onto 5-ATP-GO is chemisorption. This model also considers the bimolecular interaction involving electron exchange between the adsorbate and the adsorbent, potentially through electron-donating groups on 5-ATP-GO.[11]

3.4.2 Adsorption isotherms. The adsorption isotherm study for 5-ATP-GO towards Hg(II), Cd(II), and As(III)is essential to assess the interactions between the adsorbent and the adsorbate, so that the adsorbent performance can be optimized for real applications. As depicted in Fig. 14b, adsorption capacities of 229 ± 12, 307 ± 12, and 354 ± 8 mg for Hg(II), Cd(II), and As(III) per gram of 5-ATP-GO were obtained in this study, respectively. The adsorption capacity of 5-amino-3(2-thienyl)pyrazole (5-ATP-GO) for Hg(II) as well as for Cd(II) was moderately higher than those of 3-aminopyrazole-GO. The

higher adsorption capacity of 5-ATP-GO is explained by the presence of activated surface –NH– functional groups in aminated GO. In addition, the presence of bulky thienyl groups was effective in improving the adsorption performance by preventing the agglomeration of graphene sheets.[20] The moderate increase in the adsorption capacity of the new adsorbent for mercury and cadmium can be attributed to the hydrolysis of these materials in basic media and the formation of $(Cd(OH)^+)$[59] and water-soluble mercury complexes $(Hg(OH)_3^-$ and $Hg(OH)_4^-)$.[59] In basic environments, arsenic does not precipitate due to electrostatic repulsion, which facilitates its improved adsorption onto the surface of 5-ATP-GO.[60] Furthermore, experimental data fitting into the nonlinear form of Freundlich, Langmuir, and Sips isotherm families indicate that the actions of 5-ATP-GO correlate better with the Freundlich isotherm provided the best fit with the highest R^2 and the lowest SSE, HYBRID, and χ^2 concerning Langmuir and Sips isotherms (Table 10 and Fig. 16), and it is often used for cases of heavy metal sorption onto carbon materials. Therefore, it may be

Table 10 Nonlinear adsorption isotherm models and their parameters for the adsorption of Hg(II), Cd(II), and As(III) on GO and 5-ATP-GO

Model	Parameter	GO			5-ATP-GO		
		Hg(II)	Cd(II)	As(III)	Hg(II)	Cd(II)	As(III)
Freundlich	K_F	135.759	219.111	30.960	197.100	250.614	62.237
	n	15.143	163.986	3.934	51.530	34.876	2.514
	R^2	0.970	0.983	0.986	0.994	0.984	0.999
	SSE	1571.782	1356.486	201.305	463.182	1905.363	141.976
	HYBRID	296.233	216.558	82.168	74.559	242.243	20.454
	χ^2	8.887	6.497	2.465	2.237	7.267	0.614
Langmuir	q_m	179.972	224.982	119.264	213.522	280.082	450.952
	K_L	1.033	10.736	0.051	4.269	11.736	0.041
	R^2	0.966	0.983	0.979	0.993	0.984	0.995
	SSE	1780.853	1357.756	301.859	502.784	1955.233	721.147
	HYBRID	323.305	216.618	120.194	79.600	244.863	112.087
	χ^2	9.699	6.499	3.606	2.388	7.346	3.363
Sips	q_m	660.588	467.879	1535.290	211.344	279.403	12 598.165
	K_S	1.817×10^{-7}	1.748×10^{-5}	4.378×10^{-7}	9.171	2.001	2.058×10^{-6}
	n	0.087	0.012	0.266	23.455	8.543	0.406
	R^2	0.970	0.983	0.986	0.993	0.984	0.999
	SSE	1579.971	1356.544	203.282	521.480	1953.786	143.819
	HYBRID	445.715	324.834	124.169	122.102	366.360	31.247
	χ^2	8.914	6.497	2.483	2.442	7.327	0.625
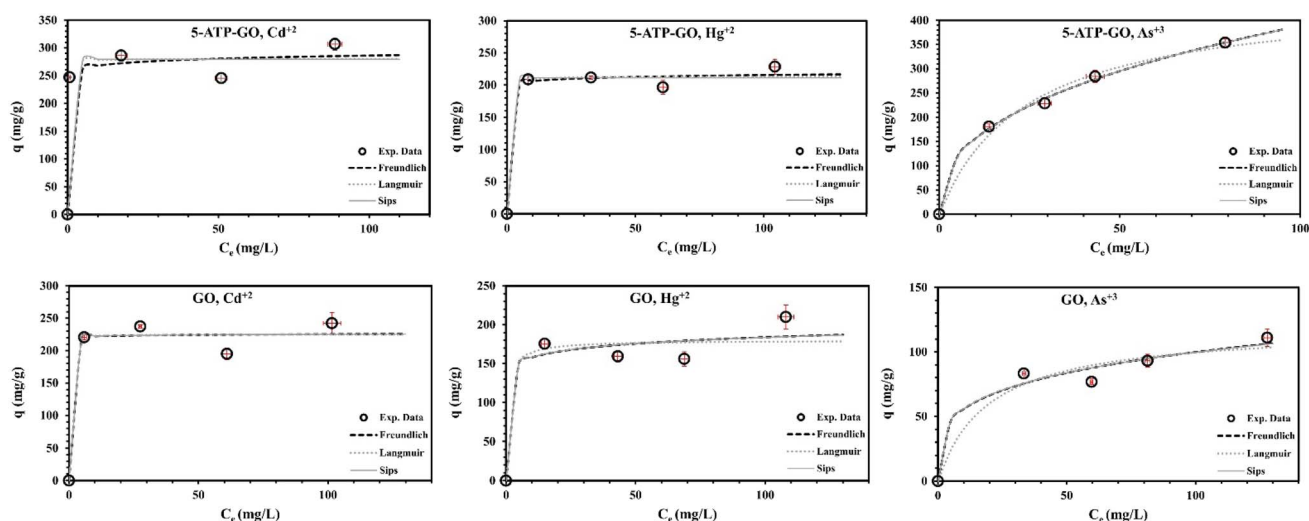
Fig. 16 Representation of the Langmuir, Freundlich, and Sips isotherm models for GO and 5-ATP-GO in nonlinear regression analysis by comparison with experimental data, for Hg(II), Cd(II), and As(III) sorption at 25 °C under optimum conditions.

supposed that the multilayer adsorption route is accomplished on the heterogeneous 5-ATP-GO surface.[40] Generally, in the Freundlich model, n (favorability) and K_F (adsorption capability) increase as q of the adsorbent and adsorption strength increase, respectively. Furthermore, all of the calculated n values exhibit greater than 1 (Table 10), signifying favorable adsorption of heavy metals on 5-ATP-GO under the conducted adsorption conditions.[63] The Freundlich constant, K_F, representing relative adsorption capacity, was determined as 197.1, 250.6, and 62.2 mg for Hg(II), Cd(II), and As(III) per gram of the adsorbent, respectively.

Based on the observed adsorption efficiencies, it is evident that sonication significantly enhanced the performance of 5-

ATP-GO. The sonication process ensures thorough dispersion of the adsorbent particles, preventing agglomeration and enhancing the exposure of active sites for heavy metal binding. This method promotes a more uniform interaction with the target ions in solution, thereby improving adsorption rates. The chosen two-hour duration was based on prior studies, which demonstrated that extended sonication optimizes these effects without degrading the adsorbent structure.

3.5 Characterization of the phases before and after Cd(II) adsorption by 5-ATP-GO

To further investigate the mechanism of adsorption and validate the chemical interactions between the adsorbent and
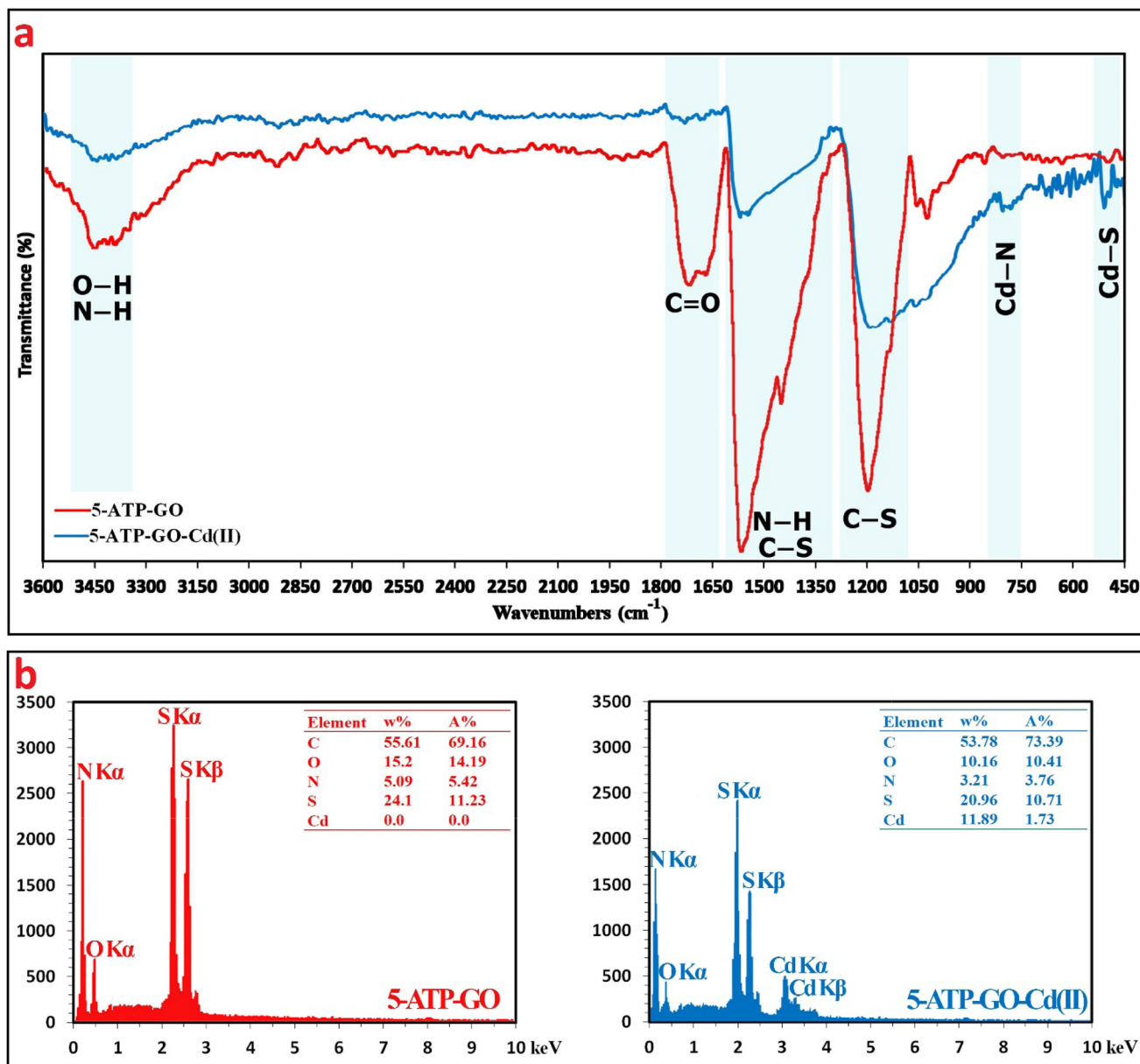
Fig. 17 (a) FTIR spectra and (b) EDX analysis of 5-ATP-GO before and after cadmium adsorption.

metal ions, cadmium (Cd(II)) was selected as a representative metal due to its relatively high adsorption capacity on 5-ATP-GO, as demonstrated in previous experiments. Among the three studied heavy metals, Cd(II) exhibited not only strong affinity toward the adsorbent surface but also consistent performance under varying conditions. Therefore, detailed characterization using FTIR spectroscopy and EDX analyses was performed to gain deeper insights into the adsorption behavior of cadmium and the functional groups involved in the process.

The FTIR spectra (Fig. 17a) revealed critical changes in the chemical structure of 5-ATP-GO after cadmium adsorption. A notable reduction in the C=O stretching vibration at 1725 cm^{-1} in the Cd-loaded sample (5-ATP-GO-Cd) compared to pristine 5-ATP-GO suggested the direct involvement of carboxyl groups in binding Cd(II). Likewise, the decreased intensities of N–H and

O–H stretching vibrations (~3400 cm^{-1}) indicated the participation of amino and hydroxyl groups through hydrogen bonding and coordination. Moreover, the appearance of distinct peaks at 509 cm^{-1} (Cd–S) and 804 cm^{-1} (Cd–N) further confirmed specific interactions of Cd(II) ions with thiol and nitrogen-containing functionalities,[64] highlighting the multi-faceted binding modes enabled by the 5-ATP modification.

EDX analysis further supported these findings by confirming the elemental composition changes upon cadmium adsorption (Fig. 17b). The pristine 5-ATP-GO contained key functional elements such as carbon (C), oxygen (O), nitrogen (N), and sulfur (S), all of which contribute to its adsorption capability. After Cd(II) adsorption, the presence of significant cadmium peaks in the EDX spectrum verified the successful sorption process. Additionally, changes in the atomic and weight

percentages of oxygen, nitrogen, and sulfur elements suggested the active participation of $-COOH$, $-OH$, $-NH_2$, and $-SH$ groups in binding cadmium ions. In particular, the strong covalent interactions between Cd(II) and thiol groups ($-SH$) confirmed the vital role of sulfur-containing functionalities in enhancing metal ion retention. These complementary FTIR and EDX results together underscore the dual contribution of both the chemical functionality introduced by 5-ATP groups and the structural characteristics of the GO-based adsorbent in achieving efficient and selective removal of cadmium ions from aqueous media.

3.6 Comparison

In order to better evaluate the performance of 5-ATP-GO, its adsorption capacity and efficiency were compared with those of other GO-based adsorbents reported in previous studies. It should be noted that making an unbiased comparison between previously studied adsorbents and the one investigated in this work is challenging due to variations in experimental conditions—such as the amount of adsorbent used, the volume of heavy metal solutions, initial ion concentrations, temperature, equilibration time, and pH. These varying parameters can significantly influence the adsorption capacity. Furthermore, some experiments were carried out under non-realistic conditions of the adsorption process such as excessively high metal ion concentration and use of adsorbent doses 10 to 500 times greater than in this study which do not reflect the practical applicability of those adsorbents.

Table 11 presents a comparison between several studies utilizing graphene oxide as a heavy metal adsorbent and the findings of the present study. Using a similar sorbent dose (10 mg) and 20 ppm initial metal ion concentrations (q_e (Hg(II)) = 91.8, q_e(Cd(II)) = 102.9, and q_e(As(III)) = 91 mg g^{-1}), Guo et al.[65] reported that the q_{max} value (the maximum capacity of adsorption) of Fe$_3$O$_4$-GS for Hg(II) and Cd(II) are 27.8 and 23.03 mg g^{-1} (approximately four times lower than those of 5-ATP-GO), respectively. A similar maximum sorption capacity for As(III) (64.2 mg g^{-1}) was reported by S. K. Kumar and S.-J. Jiang[66] for Chitosan-GO, using initial arsenic concentrations ranging from 30 to 500 mg L^{-1} and a sorbent dose of 200 mg (which is 20 times higher than that used in this study). Likewise, lower q_{max} values were reported for some other sorbents in the literature, such as amino-functionalized graphene hybrid (GO–polydopamine, q_e = 33.3 m g^{-1} at [Cd(II)]$_i$ = 50 mg L^{-1})[67] and L-cysteine-functionalized exfoliated GO (q_e = 79.36 mg g^{-1} at [Hg(II)]$_i$ = 10 mg L^{-1}).[68] It should be noted that the adsorbent doses used in those studies were significantly higher than that used in the present work. However, 5-ATP-GO exhibited a lower maximum adsorption capacity (q_e (Hg(II)) = 212.5 and q_e(Cd(II)) = 280.1 mg g^{-1}) compared to 3-aminopyrazole-GO (q_e (Hg(II)) = 227.3 and q_e(Cd(II)) = 285.7 mg g^{-1}) reported in our previous study,[19] while 5-ATP-GO demonstrated a faster adsorption rate, reaching equilibrium within 30 minutes, compared to 60 minutes for 3-aminopyrazole-GO.

Although the adsorption capacity of 5-ATP-GO is lower than that of some previously reported sorbents—such as GO (q_e(Cd(II)) = 1531.7 mg g^{-1}),[69] IT-PRGO (q_e(Hg(II)) = 624 mg g^{-1}),[70]

Table 11 Comparison of the adsorption capacity with experimental conditions of different adsorbents for Hg(II), Cd(II), and As(III) adsorption

Adsorbent	pH	m (mg)	C_0 (mg L^{-1})	T (°C)	q_{max} (mg g^{-1})			Reference
					Hg(II)	Cd(II)	As(III)	
MBT-GO	5.9			RT	107.52	—	—	74
GO/2-PTSC	5.0	6	20	RT	555.00	—	—	75
GO and GO/CS	4.0			25	381 and 187	—	—	76
3DGON	4.5			21	35	—	—	77
GO/Fe–Mn	7.0			25	32.9	—	—	17
ITPRGO	5.0			25	624			70
FGOCA	7.0			25	374	181	—	62
3D-GO foam	10.0			RT	—	252.50	—	78
GO-polydopamine	5.2–6.8			RT	—	33.30	—	79
GO-DPA	8.0			RT	—	253.00	—	80
3D-SRGO	6.0			25	—	234.80	—	69
MMSP-GO	7.1			30	—	167.00	—	81
GO-starch	5.8			30	—	43.20	—	82
Chitosan-GO	8.7–10.8			RT	—	—	64.20	68
M-GO	7.0			25	—	—	42.9	83
M-rGO	7.0			25	—	—	29.8	83
PG-Fe$_3$O$_4$	7.0			25	—	—	104	84
NZVI–RGO	7.0			25	—	—	33.83	85
GIAMO-1	7.0			20	—	—	42.28	86
GO–ZrO(OH)$_2$	7.0			25	—	—	95.15	87
3-Aminopyrazole-GO	8.3/8.8/7.6			RT	227.27	285.70	131.58	19
GO	8/8.7/7.7			RT	179.97	224.98	119.26	This work
5-ATP-GO	7.9/8.2/7.2			RT	213.52	280.08	450.95	This work

and Fe$_3$O$_4$–Polypyrrole-GO (q_e(Hg(II)) = 400 mg g^{-1})[71]—it is still considered a more promising sorbent due to its significantly lower required dose (0.2 mg L^{-1}) and excellent adsorption rate (30 minutes). Moreover, the maximum adsorption capacity for arsenic reported in this study (q_e(As(III)) = 450.95 mg g^{-1}) is higher than those reported in recent studies. The higher sorption capacity of As(III) can be attributed to its smaller hydrated ionic radius (72 pm), which makes it more easily trapped within the pores of the adsorbent compared to Hg(II) and Cd(II).

Despite the fact that some of the aforementioned sorbents involve multi-step synthesis procedures, the substitutional functionalization used for 5-ATP-GO offers a simpler and more economically viable alternative. In summary, 5-ATP-GO demonstrates significant advantages in terms of cost-effectiveness, operational simplicity, and efficiency, as it requires a small sorbent dose to effectively remove cadmium, mercury, and arsenic from wastewater within a short contact time.

3.7 Competing between ions together and adsorbent regeneration

Investigating the effect of co-ions on adsorbents towards metal ion uptake is necessary as they usually co-exist and make competitive adsorption in aquatic sources. The results revealed that the coexisting ions had slight interventions on the q of Hg(II), Cd(II), and As(III), which indicates that the efficiency of adsorption of the ions declines weakly under competitive conditions. This finding additionally demonstrates the latent use of this adsorbent to heavy metal uptake in actual processes (Table 12). The adsorption efficiency order observed in this study, with cadmium exhibiting the highest removal rate followed by mercury and arsenic, can be attributed to several physicochemical factors. Cadmium's smaller ionic radius and higher hydration energy facilitate stronger electrostatic interactions with the negatively charged and functionalized sites on 5-ATP-GO. In contrast, mercury, despite its high toxicity, exhibits a slightly lower affinity due to its larger ionic radius and lower charge density. Arsenic shows the least adsorption efficiency, likely because of its different ionic state (As(III)), which hinders effective bonding with the functional groups present on the adsorbent. These variations underscore the significant role of ionic properties such as radius, charge density, and hydration in determining adsorption selectivity. Moreover, the sulfur and
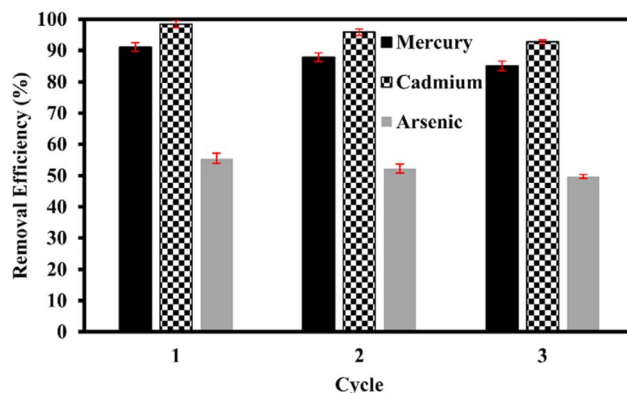

Fig. 18 The number of adsorption–desorption cycles of Cd(II) Hg(II), and As(III) on 5-ATO-GO at 1.0 M HCl concentration.

nitrogen groups on 5-ATP-GO likely contribute to preferential binding through specific chemisorption interactions, enhancing the removal efficiency of metals with higher affinity to these sites.

Moreover, it is important to appraise the reusability of the adsorbent after adsorbing metal ions, as it significantly impacts the cost of removing heavy metals from contaminated waste. Additionally, disposal of the adsorbent can have contrary ecological effects. In this study, desorption investigation shows that 5-ATP-GO maintained its performance efficiency after the third adsorption–desorption sequence, with only a slight decrease in cadmium, mercury, and arsenic uptake (Fig. 18). This could be attributable to the excess regaining of binding sites of metal ions after steps of desorption, combined with the use of the appropriate eluent. This significantly increases the recyclability of the adsorbent. This outstanding result shows that 5-ATP-GO has worthy reusability and stability, which can aid decreasing the amount of used adsorbent. By recycling, we can help combat the climate crisis by reducing the need for raw materials and limiting waste going into landfills.

In addition to evaluating adsorption under competitive ion conditions, assessing the reusability of the adsorbent after metal ion uptake is crucial, as it significantly affects the overall cost-effectiveness of heavy metal removal from wastewater. Improper disposal of the used adsorbent may lead to adverse environmental consequences. In this study, the desorption investigation showed that 5-ATP-GO retained its efficiency even after three consecutive adsorption–desorption cycles, with only a minimal reduction in the uptake of metal ions (Fig. 18). This retention in performance can be attributed to the effective regeneration of metal-binding sites during the desorption steps, facilitated by the use of an appropriate eluent. This notably enhances the reusability potential of the adsorbent. This remarkable outcome demonstrates that 5-ATP-GO possesses excellent reusability and structural stability, which helps reduce the quantity of adsorbent required in repeated cycles. Recycling the adsorbent contributes to mitigating environmental challenges by minimizing the demand for virgin materials and reducing the volume of waste directed to landfills.

Table 12 Comparison of the adsorption capacity of the heavy metal ions at pH = 8.0 and the concentration of each metal ion is 20 ppm at room temperature

Ions	Noncompetitive adsorption		Competitive adsorption	
	GO	5-ATP-GO	GO	5-ATP-GO
Cd(II)	73.6	78.1	66.8	67.9
Hg(II)	56.3	86.7	55.4	77.3
As(III)	26.2	32.1	23.7	27.4

3.8 Application of 5-ATP-GO in real-water sample treatment

To evaluate the 5-ATP-GO efficiency under real conditions, the studies of adsorption were carried out applying Caspian Sea (Iran) water, which was contaminated with Cd(ɪɪ), and matched with GO and commercial activated carbon (CAC). The Caspian Sea is a complex solution of diverse ions that compete for vacant adsorbent sites. Moreover, the existence of organic materials in the sea limits Cd(ɪɪ) mobility and makes the adsorption of Cd(ɪɪ) onto the adsorbent difficult.[70] However, the results of experiments demonstrated that the q value of 5-ATP-GO was only a little influenced by such a complex water system (experimental conditions: $C_0 = 50$ ppm, $V = 100$ mL, and $m = 10$). By comparing the removal efficiency of 5-ATP-GO with GO in this real application study, it was found that 5-ATP-GO (86.7%) has a greater removal efficiency than that of GO (57.8%). Furthermore, the removal efficiency of CAC (37.3%) was the worst for cadmium adsorption. The reduced surface area in 5-ATP-GO owing to the addition of an extra functional agent and the obstruction of some pores throughout functionalization by 5-amino-3(2-thienyl)pyrazole does not seem to affect the distinction of the prepared sorbent despite the accessibility of the vigorous functional assemblies such as amine and sulfur groups on the 5-ATP-GO surface. In addition, it was considered that the outcome of the actual sample study applying sea water (pH ∼ 8.3) is notably consistent with the pH study that the cadmium capacity of adsorption is ∼90% at a pH of 8.3. This discloses that the cadmium adsorption capacity of 5-ATP-GO depends heavily on the pH. This distinguished result shows that this material is potent for trapping cadmium in the existing water processes.

4 Conclusions

A 3D graphene-based adsorbent functionalized with several tie functionalities such as oxygen, sulfur and amine groups was synthesized successfully using amide bonding of 5-amino-3(2-thienyl)pyrazole on GO *via* a substitution reaction. The obtained material, 5-ATP-GO, demonstrated high efficiency for the adsorption of Hg(ɪɪ), Cd(ɪɪ), and As(ɪɪɪ) ions from aqueous solutions. The structural modification introduced abundant active sites and diverse surface chemistries, which significantly enhanced the selectivity and binding capacity of the adsorbent. To optimize the adsorption process conditions, a central composite design under response surface methodology, CCD/RSM, was employed, focusing on the pH, initial metal ion concentration, and adsorbent dosage. The results of ANOVA confirmed that quadratic models ($R^2 > 0.99$, $p < 0.05$) were most appropriate for predicting the optimal adsorption performance. The optimum parameters were determined to be a pH of 7.25–8.55, an adsorbent dosage of 10–10.50 g L^{-1}, and an initial metal ion concentration of 43.45–49.66 mg L^{-1}. To gain deeper insights into the adsorption mechanism, the kinetic and isotherm models were evaluated. They showed that the adsorption process followed a pseudo-second-order kinetic model and fitted well to the Freundlich isotherm, indicating a heterogeneous chemisorption mechanism. The maximum

adsorption capacities of 5-ATP-GO were 213.5, 280.1, and 450.9 mg g^{-1} for Hg(ɪɪ), As(ɪɪɪ), and Cd(ɪɪ), respectively—significantly higher than those of pristine GO. Furthermore, under competitive adsorption conditions, cations with a higher charge density and smaller hydrated ionic radii exhibited a stronger tendency to interact with the functionalized surface of 5-ATP-GO, following the selectivity order Cd(ɪɪ) > Hg(ɪɪ) > As(ɪɪɪ). At low pollutant concentrations (*e.g.*, 0.2 mg L^{-1}), the adsorbent exhibited rapid uptake (>75% removal in 30 min) and excellent reusability (>90% capacity retained after three cycles). Moreover, compared to other reported sorbents, 5-ATP-GO showed higher q and better regeneration efficiency, particularly for Cd(ɪɪ), under similar experimental conditions. Entering the final phase, the applicability of 5-ATP-GO was tested in a real-world scenario using Caspian Sea water samples spiked with cadmium. Despite the complex ionic composition and organic matter in seawater, the material maintained high adsorption efficiency. The q value of 5-ATP-GO (433.5 mg g^{-1}) exceeded those of commercial activated carbon (CAC, 186.5 mg g^{-1}) and GO (289 mg g^{-1}), even under low-dose conditions. In conclusion, the developed 5-ATP-GO adsorbent demonstrates high selectivity, exceptional adsorption capacity, and notable reusability, making it a promising candidate for addressing the challenges of heavy metal pollution in water resources. Furthermore, the scalable and low-cost strategy used for functionalizing 3D graphene provides a flexible platform adaptable to various environmental remediation needs.

Conflicts of interest

The authors declare that there are no conflicts of interest regarding the publication of this manuscript.

Abbreviation

5-ATP-GO	5-Amino-3(2-thienyl)pyrazole-modified graphene oxide
ANOVA	Analysis of variance
BET	Brunauer–Emmett–Teller
C_0	Concentrations at beginning
CAC	Commercial activated carbon
CCD	Central composite design
CCD	Central composite design
C_t	Concentrations at time t
DMF	N,N-dimethylformamide
DMSO	Dimethyl sulfoxide
DOE	Design of experiments
FE-SEM	Field emission scanning electron microscopy
FTIR	Fourier transform infrared spectroscopy
GF-AAS	Graphite furnace atomic absorption spectroscopy instrument
GO	Graphene oxide
GRG	Generalized reduced gradient
HYBRID	Hybrid fractional error function
L	Volume of solution
m	Adsorbent mass

MCM-41	Mobil composition of matter no. 41
PFO	Pseudo first order
PSO	Pseudo second order
q	Adsorption capacity
q_{exp}	Capacity of adsorption
R^2	Correlation coefficient
rGO	Reduced graphene oxide
RT	Room temperature
SBA-15	Santa barbara amorphous-15
SD	Standard deviation
SSE	Sum of squares error
TG	Thermo gravimetric
THF	Tetrahydrofuran
XRD	X-ray diffraction
ZP	Zeta-potential
χ^2	chi error

Data availability

The authors confirm that the data supporting the findings of this study are available within the article. Additional data are available from the corresponding author upon reasonable request.

Acknowledgements

References

1 J. Bayuo, A. B. Alayande, K. M. Mtei and M. J. Rwiza, Biochar-based Technology in Water and Wastewater Treatment, *Low Cost Water and Wastewater Treatment Systems: Conventional and Recent Advances*, Elsevier, 2025, pp. 153–194.

2 J. Bayuo, K. B. Pelig-Ba and M. A. Abukari, Adsorptive removal of chromium (VI) from aqueous solution unto groundnut shell, *Appl. Water Sci.*, 2019, 9, 107.

3 Y. Lu, B. Jiang, L. Fang, F. Ling, J. Gao, F. Wu and X. Zhang, High performance NiFe layered double hydroxide for methyl orange dye and Cr(VI) adsorption, *Chemosphere*, 2016, 152, 415–422.

4 D. Zhu, Y. Cheng, B. Xue, Y. Jiang and C. Wei, Coal gasification fine slag as a low-cost adsorbent for adsorption and desorption of humic acid, *Silicon*, 2020, 12, 1547–1556.

5 J. Bayuo, M. J. Rwiza, J. W. Choi, K. N. Njau and K. M. Mtei, Recent and sustainable advances in phytoremediation of heavy metals from wastewater using aquatic plant species: Green approach, *J. Environ. Manage.*, 2024, 370, 122523.

6 Z. Tang, Z. Qiu, S. Lu and X. Shi, Functionalized layered double hydroxide applied to heavy metal ions absorption: A review, *Nanotechnol. Rev.*, 2020, 9, 800–819.

7 R. Yousef, H. Qiblawey and M. H. El-Naas, Adsorption as a process for produced water treatment: a review, *Processes*, 2020, 8, 1657.

8 J. Bayuo, M. J. Rwiza, M. Sillanpää and K. M. Mtei, Removal of heavy metals from binary and multicomponent adsorption systems using various adsorbents–a systematic review, *RSC Adv.*, 2023, 13, 13052–13093.

9 H. SadeghG. A. Ali, *Research anthology on synthesis, characterization, and applications of nanomaterials*, IGI Global2021pp. 1230–1240.

10 J. Bayuo, M. J. Rwiza and K. M. Mtei, Adsorption and desorption ability of divalent mercury from an interactive bicomponent sorption system using hybrid granular activated carbon, *Environ. Monit. Assess.*, 2023, 195, 935.

11 T. Liu, M. Yang, T. Wang and Q. Yuan, Prediction strategy of adsorption equilibrium time based on equilibrium and kinetic results to isolate taxifolin, *Ind. Eng. Chem. Res.*, 2012, 51, 454–463.

12 M. J. Sweetman, S. May, N. Mebberson, P. Pendleton, K. Vasilev, S. E. Plush and J. D. Hayball, Activated carbon, carbon nanotubes and graphene: materials and composites for advanced water purification, *C*, 2017, 3, 18–47.

13 A. Walcarius and L. Mercier, Mesoporous organosilica adsorbents: nanoengineered materials for removal of organic and inorganic pollutants, *J. Mater. Chem.*, 2010, 20, 4478–4511.

14 S. Gadipelli and Z. X. Guo, Graphene-based materials: Synthesis and gas sorption, storage and separation, *Prog. Mater. Sci.*, 2015, 69, 1–60.

15 K. C. Kemp, H. Seema, M. Saleh, N. H. Le, K. Mahesh, V. Chandra and K. S. Kim, Environmental applications using graphene composites: water remediation and gas adsorption, *Nanoscale*, 2013, 5, 3149–3171.

16 S. Kabiri, D. N. Tran, M. A. Cole and D. Losic, Functionalized three-dimensional (3D) graphene composite for high efficiency removal of mercury, *Environ. Sci.: Water Res. Technol.*, 2016, 2, 390–402.

17 W. Gao, M. Majumder, L. B. Alemany, T. N. Narayanan, M. A. Ibarra, B. K. Pradhan and P. M. Ajayan, Engineered graphite oxide materials for application in water purification, *ACS Appl. Mater. Interfaces*, 2011, 3, 1821–1826.

18 S. Kabiri, D. N. Tran, S. Azari and D. Losic, Graphene-diatom silica aerogels for efficient removal of mercury ions from water, *ACS Appl. Mater. Interfaces*, 2015, 7, 11815–11823.

19 M. Alimohammady, M. Jahangiri, F. Kiani and H. Tahermansouri, Highly efficient simultaneous adsorption of Cd(II), Hg(II) and As(III) ions from aqueous solutions by modification of graphene oxide with 3-aminopyrazole: central composite design optimization, *New J. Chem.*, 2017, 41, 8905–8919.

20 M. Alimohammady and M. Ghaemi, Adsorptive removal of Hg^{2+} from aqueous solutions using amino phenyl-pyrazole-functionalized graphene oxide, *Carbon Lett.*, 2020, 30, 493–508.

21 H. Tian, J. Guo, Z. Pang, M. Hu and J. He, A sulfur, nitrogen dual-doped porous graphene nanohybrid for ultraselective Hg(II) separation over Pb(II) and Cu(II), *Nanoscale*, 2020, 12, 16543–16555.

22 S. Witomska, Z. Liu, W. Czepa, A. Aliprandi, D. Pakulski, P. Pawluć, A. Ciesielski and P. Samorì, Graphene oxide hybrid with sulfur–nitrogen polymer for high-performance pseudocapacitors, *J. Am. Chem. Soc.*, 2018, **141**, 482–487.

23 G. Kotan, F. Kardaş, Ö. A. Yokuş, O. Akyıldırım, H. Saral, T. Eren, M. L. Yola and N. Atar, A novel determination of curcumin via Ru@Au nanoparticle decorated nitrogen and sulfur-functionalized reduced graphene oxide nanomaterials, *Anal. Methods*, 2016, **8**, 401–408.

24 P. H. Wadekar, R. V. Khose, D. A. Pethsangave and S. Some, One-Pot Synthesis of Sulfur and Nitrogen Co-Functionalized Graphene Material using Deep Eutectic Solvents for Supercapacitors, *ChemSusChem*, 2019, **12**, 3326–3335.

25 D. N. Tran, S. Kabiri and D. Losic, A green approach for the reduction of graphene oxide nanosheets using non-aromatic amino acids, *Carbon*, 2014, **76**, 193–202.

26 H. Dan, N. Li, X. Xu, Y. Gao, Y. Huang, M. Akram, W. Yin, B. Gao and Q. Yue, Mechanism of sonication time on structure and adsorption properties of 3D peanut shell/graphene oxide aerogel, *Sci. Total Environ.*, 2020, **739**, 139983.

27 E. Khalili Drermani and R. Afzalzadeh, Experimental comparison of the effects of the two designed probes for exfoliation of graphene by sonication, *Sci. Rep.*, 2024, **14**, 22682.

28 G. T. T. Le, N. Chanlek, J. Manyam, P. Opaprakasit, N. Grisdanurak and P. Sreearunothai, Insight into the ultrasonication of graphene oxide with strong changes in its properties and performance for adsorption applications, *Chem. Eng. J.*, 2019, **373**, 1212–1222.

29 M. Sandhya, D. Ramasamy, K. Sudhakar, K. Kadirgama and W. Harun, Ultrasonication an intensifying tool for preparation of stable nanofluids and study the time influence on distinct properties of graphene nanofluids–A systematic overview, *Ultrason. Sonochem.*, 2021, **73**, 105479.

30 L. Shen, S. Pang, M. Zhong, Y. Sun, A. Qayum, Y. Liu, A. Rashid, B. Xu, Q. Liang and H. Ma, A comprehensive review of ultrasonic assisted extraction (UAE) for bioactive components: Principles, advantages, equipment, and combined technologies, *Ultrason. Sonochem.*, 2023, **101**, 106646.

31 F. W. Breyfogle III, *Statistical Methods for Testing, Development, and Manufacturing*, John Wiley & Sons, 1992.

32 J. Bayuo, M. A. Abukari and K. B. Pelig-Ba, Optimization using central composite design (CCD) of response surface methodology (RSM) for biosorption of hexavalent chromium from aqueous media, *Appl. Water Sci.*, 2020, **10**, 1–12.

33 S. Somadasan, G. Subramaniyan, M. S. Athisayaraj and S. K. Sukumaran, Central Composite Design: An Optimization Tool for Developing Pharmaceutical Formulations, *J. Young Pharm.*, 2024, **16**, 400–409.

34 J. Bayuo, M. Rwiza, M. A. Abukari, K. B. Pelig-Ba and K. Mtei, Modeling and optimization of independent factors influencing lead (II) biosorption from aqueous systems: A statistical approach, *Sci. Afr.*, 2022, **16**, e01270.

35 J. Bayuo, M. J. Rwiza and K. M. Mtei, Optimization of divalent mercury removal from synthetic wastewater using desirability function in central composite design of response surface methodology, *J. Environ. Health Sci. Eng.*, 2024, **22**, 209–227.

36 N. Szpisják-Gulyás, A. N. Al-Tayawi, Z. H. Horváth, Z. László, S. Kertész and C. Hodúr, Methods for experimental design, central composite design and the Box–Behnken design, to optimise operational parameters: A review, *Acta Aliment.*, 2023, **52**, 521–537.

37 M. Alimohammady, M. Jahangiri, F. Kiani and H. Tahermansouri, Competent heavy metal adsorption by modified MWCNTs and optimization process by experimental design, *J. Environ. Eng.*, 2018, **144**, 202–224.

38 M. Alimohammady, M. Jahangiri, F. Kiani and H. Tahermansouri, Design and evaluation of functionalized multi-walled carbon nanotubes by 3-aminopyrazole for the removal of Hg (II) and As (III) ions from aqueous solution, *Res. Chem. Intermed.*, 2018, **44**, 69–92.

39 M. Alimohammady, M. Jahangiri, F. Kiani and H. Tahermansouri, Preparation and characterization of functionalized MWCNTs-COOH with 3-amino-5-phenylpyrazole as an adsorbent and optimization study using central composite design, *Carbon Lett.*, 2019, **29**, 1–20.

40 A. Bonilla-Petriciolet, D. I. Mendoza-Castillo and H. E. Reynel-Ávila, *Adsorption Processes for Water Treatment and Purification*, Springer, 2017.

41 A. Esmaeilian, A. Mahdavi Mazdeh, H. Ghaforian and A. Liaghat, A novel nanopore biopolymer multi adsorbent for simultaneous removal of anionic and cationic mixtures, *Desalination Water Treat.*, 2015, **53**, 2235–2248.

42 J. Bayuo, M. J. Rwiza, J. W. Choi, K. M. Mtei, A. Hosseini-Bandegharaei and M. Sillanpää, Adsorption and desorption processes of toxic heavy metals, regeneration and reusability of spent adsorbents: economic and environmental sustainability approach, *Adv. Colloid Interface Sci.*, 2024, **329**, 103196.

43 J. Bayuo, M. J. Rwiza, K. M. Mtei and J. W. Choi, *Adsorptive Removal of Heavy Metals from Wastewater Using Low-Cost Adsorbents Derived from Agro-Based Materials, Heavy Metal Remediation: Sustainable Nexus Approach*, Springer, 2024, pp. 237–271.

44 J. Bayuo, M. J. Rwiza, J. W. Choi, M. Sillanpää and K. M. Mtei, Optimization of desorption parameters using response surface methodology for enhanced recovery of arsenic from spent reclaimable activated carbon: Eco-friendly and sorbent sustainability approach, *Ecotoxicol. Environ. Saf.*, 2024, **280**, 116550.

45 H. Ghoveisi, J. Farhoudi, M. Omid and A. M. Mazdeh, Comparison of different methods for linear regression of pseudo second order adsorption kinetics of cadmium, *J. Civ. Eng. Urban.*, 2013, **3**, 73–76.

46 M. Deng, Y. Huang, X. Zhang, Z. Feng, J. Gou and B. Sun, Preparation of a novel chelating resin bearing amidinothiourea moieties and its removal properties for

Hg (II) ions in aqueous solution, *Sep. Sci. Technol.*, 2016, **51**, 1499–1508.

47 M. Wojtoniszak, X. Chen, R. J. Kalenczuk, A. Wajda, J. Łapczuk, M. Kurzewski, M. Drozdzik, P. K. Chu and E. Borowiak-Palen, Synthesis, dispersion, and cytocompatibility of graphene oxide and reduced graphene oxide, *Colloids Surf., B*, 2012, **89**, 79–85.

48 E. S. Orth, J. E. Fonsaca, S. H. Domingues, H. Mehl, M. M. Oliveira and A. J. Zarbin, Targeted thiolation of graphene oxide and its utilization as precursor for graphene/silver nanoparticles composites, *Carbon*, 2013, **61**, 543–550.

49 T. S. Qureshi and D. K. Panesar, Impact of graphene oxide and highly reduced graphene oxide on cement based composites, *Constr. Build. Mater.*, 2019, **206**, 71–83.

50 S. Thakur, G. Das, P. K. Raul and N. Karak, Green one-step approach to prepare sulfur/reduced graphene oxide nanohybrid for effective mercury ions removal, *J. Phys. Chem. C*, 2013, **117**, 7636–7642.

51 Q. Lian, Z. U. Ahmad, D. D. Gang, M. E. Zappi, D. L. B. Fortela and R. Hernandez, The effects of carbon disulfide driven functionalization on graphene oxide for enhanced Pb (II) adsorption: Investigation of adsorption mechanism, *Chemosphere*, 2020, **248**, 126078.

52 A. Shahzad, W. Miran, K. Rasool, M. Nawaz, J. Jang, S.-R. Lim and D. S. Lee, Heavy metals removal by EDTA-functionalized chitosan graphene oxide nanocomposites, *RSC Adv.*, 2017, **7**, 9764–9771.

53 A. M. Dimiev and S. Eigler, *Graphene Oxide: Fundamentals and Applications*, John Wiley & Sons, 2016.

54 I. Tantis, A. Bakandritsos, D. Zaoralova, M. Medveď, P. Jakubec, J. Havlakova, R. Zbořil and M. Otyepka, Covalently Interlinked Graphene Sheets with Sulfur-Chains Enable Superior Lithium–Sulfur Battery Cathodes at Full-Mass Level, *Adv. Funct. Mater.*, 2021, **31**, 2101326.

55 B. Z. Can, R. Boncukcuoglu, A. E. Yilmaz and B. A. Fil, Effect of some operational parameters on the arsenic removal by electrocoagulation using iron electrodes, *J. Environ. Health Sci. Eng.*, 2014, **12**, 1–10.

56 Y. m. Liang, M. Jun and W. Liu, Enhanced removal of lead (II) and cadmium (II) from water in alum coagulation by ferrate (VI) pretreatment, *Water Environ. Res.*, 2007, **79**, 2420–2426.

57 M. Anbia and S. Amirmahmoodi, Removal of Hg (II) and Mn (II) from aqueous solution using nanoporous carbon impregnated with surfactants, *Arab. J. Chem.*, 2016, **9**, S319–S325.

58 C. G. Rocha, D. A. M. Zaia, R. V. da Silva Alfaya and A. A. da Silva Alfaya, Use of rice straw as biosorbent for removal of Cu (II), Zn (II), Cd (II) and Hg (II) ions in industrial effluents, *J. Hazard. Mater.*, 2009, **166**, 383–388.

59 M. J. Shadbad, A. Mohebbi and A. Soltani, Mercury (II) removal from aqueous solutions by adsorption on multi-walled carbon nanotubes, *Korean J. Chem. Eng.*, 2011, **28**, 1029–1034.

60 M. Moronshing, A. Sah, V. Kalyani and C. Subramaniam, Nanostructured carbon florets as scavenger of As^{3+}, Cr^{6+}, Cd^{2+}, and Hg^{2+} for water remediation, *ACS Appl. Nano Mater.*, 2019, **3**, 468–478.

61 J. Bayuo, M. J. Rwiza and K. M. Mtei, Modeling and optimization of trivalent arsenic removal from wastewater using activated carbon produced from maize plant biomass: a multivariate experimental design approach, *Biomass Convers. Biorefin.*, 2024, **14**, 24809–24832.

62 F. Arshad, M. Selvaraj, J. Zain, F. Banat and M. A. Haija, Polyethylenimine modified graphene oxide hydrogel composite as an efficient adsorbent for heavy metal ions, *Sep. Purif. Technol.*, 2019, **209**, 870–880.

63 M. Eftekhari, M. Akrami, M. Gheibi, H. Azizi-Toupkanloo, A. M. Fathollahi-Fard and G. Tian, Cadmium and copper heavy metal treatment from water resources by high-performance folic acid-graphene oxide nanocomposite adsorbent and evaluation of adsorptive mechanism using computational intelligence, isotherm, kinetic, and thermodynamic analyses, *Environ. Sci. Pollut. Res.*, 2020, **27**, 43999–44021.

64 Y. Bian, Z.-Y. Bian, J.-X. Zhang, A.-Z. Ding, S.-L. Liu and H. Wang, Effect of the oxygen-containing functional group of graphene oxide on the aqueous cadmium ions removal, *Appl. Surf. Sci.*, 2015, **329**, 269–275.

65 X. Guo, B. Du, Q. Wei, J. Yang, L. Hu, L. Yan and W. Xu, Synthesis of amino functionalized magnetic graphenes composite material and its application to remove Cr (VI), Pb (II), Hg (II), Cd (II) and Ni (II) from contaminated water, *J. Hazard. Mater.*, 2014, **278**, 211–220.

66 A. S. K. Kumar and S.-J. Jiang, Chitosan-functionalized graphene oxide: A novel adsorbent an efficient adsorption of arsenic from aqueous solution, *J. Environ. Chem. Eng.*, 2016, **4**, 1698–1713.

67 Z. Dong, D. Wang, X. Liu, X. Pei, L. Chen and J. Jin, Bio-inspired surface-functionalization of graphene oxide for the adsorption of organic dyes and heavy metal ions with a superhigh capacity, *J. Mater. Chem. A*, 2014, **2**, 5034–5040.

68 A. S. K. Kumar and S.-J. Jiang, Preparation and characterization of exfoliated graphene oxide–L-cystine as an effective adsorbent of Hg (II) adsorption, *RSC Adv.*, 2015, **5**, 6294–6304.

69 Y. Zhang, W. Peng, L. Xia and S. Song, Adsorption of Cd (II) at the Interface of water and graphene oxide prepared from flaky graphite and amorphous graphite, *J. Environ. Chem. Eng.*, 2017, **5**, 4157–4164.

70 F. S. Awad, K. M. AbouZeid, W. M. A. El-Maaty, A. M. El-Wakil and M. S. El-Shall, Efficient removal of heavy metals from polluted water with high selectivity for mercury (II) by 2-imino-4-thiobiuret–partially reduced graphene oxide (IT-PRGO), *ACS Appl. Mater. Interfaces*, 2017, **9**, 34230–34242.

71 P. L. Yap, S. Kabiri, D. N. Tran and D. Losic, Multifunctional binding chemistry on modified graphene composite for selective and highly efficient adsorption of mercury, *ACS Appl. Mater. Interfaces*, 2018, **11**, 6350–6362.

72 S. Tabari, S. S. S. Saravi, G. A. Bandany, A. Dehghan and M. Shokrzadeh, Heavy metals (Zn, Pb, Cd and Cr) in fish, water and sediments sampled form Southern Caspian Sea, Iran, *Toxicol. Ind. Health*, 2010, **26**, 649–656.

73 J. Bayuo, K. Mtei and M. Rwiza, Applicability of bio-adsorbents synthesized from maize/corn plant residues for heavy metals removal from aquatic environments: an insight review, *EQA–Int. J. Environ. Qual.*, 2023, **56**, 15.

74 A. S. K. Kumar, S.-J. Jiang and W.-L. Tseng, Facile synthesis and characterization of thiol-functionalized graphene oxide as effective adsorbent for Hg (II), *J. Environ. Chem. Eng.*, 2016, **4**, 2052–2065.

75 A. Tadjarodi, S. Moazen Ferdowsi, R. Zare-Dorabei and A. Barzin, Highly efficient ultrasonic-assisted removal of Hg(II) ions on graphene oxide modified with 2-pyridinecarboxaldehyde thiosemicarbazone: Adsorption isotherms and kinetics studies, *Ultrason. Sonochem.*, 2016, **33**, 118–128.

76 N. M. Bandaru, N. Reta, H. Dalal, A. V. Ellis, J. Shapter and N. H. Voelcker, Enhanced adsorption of mercury ions on thiol derivatized single wall carbon nanotubes, *J. Hazard. Mater.*, 2013, **261**, 534–541.

77 Q. Wang, D. Kim, D. D. Dionysiou, G. A. Sorial and D. Timberlake, Sources and remediation for mercury contamination in aquatic systems—a literature review, *Environ. Pollut.*, 2004, **131**, 323–336.

78 Y. Lei, F. Chen, Y. Luo and L. Zhang, Synthesis of three-dimensional graphene oxide foam for the removal of heavy metal ions, *Chem. Phys. Lett.*, 2014, **593**, 122–127.

79 A. B. Đukić, K. R. Kumrić, N. S. Vukelić, M. S. Dimitrijević, Z. D. Baščarević, S. V. Kurko and L. L. Matović, Simultaneous removal of Pb²⁺, Cu²⁺, Zn²⁺ and Cd²⁺ from highly acidic solutions using mechanochemically synthesized montmorillonite–kaolinite/TiO₂ composite, *Appl. Clay Sci.*, 2015, **103**, 20–27.

80 R. Zare-Dorabei, S. M. Ferdowsi, A. Barzin and A. Tadjarodi, Highly efficient simultaneous ultrasonic-assisted adsorption of Pb(II), Cd(II), Ni(II) and Cu(II) ions from aqueous solutions by graphene oxide modified with 2, 2′-dipyridylamine: central composite design optimization, *Ultrason. Sonochem.*, 2016, **32**, 265–276.

81 Y. Wang, S. Liang, B. Chen, F. Guo, S. Yu and Y. Tang, Synergistic removal of Pb (II), Cd (II) and humic acid by Fe3O4@ mesoporous silica-graphene oxide composites, *PLoS One*, 2013, **8**, 65634–65638.

82 Z. Wang, X. Zhang, X. Wu, J.-G. Yu, X.-Y. Jiang, Z.-L. Wu and X. Hao, Soluble starch functionalized graphene oxide as an efficient adsorbent for aqueous removal of Cd (II): The adsorption thermodynamic, kinetics and isotherms, *J. Sol-gel Sci. Technol.*, 2017, **82**, 440–449.

83 Y. Yoon, W. K. Park, T.-M. Hwang, D. H. Yoon, W. S. Yang and J.-W. Kang, Comparative evaluation of magnetite–graphene oxide and magnetite-reduced graphene oxide composite for As (III) and As (V) removal, *J. Hazard. Mater.*, 2016, **304**, 196–204.

84 B. K. Kang, B. S. Lim, Y. Yoon, S. H. Kwag, W. K. Park, Y. H. Song, W. S. Yang, Y.-T. Ahn, J.-W. Kang and D. H. Yoon, Efficient removal of arsenic by strategically designed and layer-by-layer assembled PS@ + rGO@ GO@ Fe3O4 composites, *J. Environ. Manage.*, 2017, **201**, 286–293.

85 C. Wang, H. Luo, Z. Zhang, Y. Wu, J. Zhang and S. Chen, Removal of As (III) and As (V) from aqueous solutions using nanoscale zero valent iron-reduced graphite oxide modified composites, *J. Hazard. Mater.*, 2014, **268**, 124–131.

86 S. Maji, A. Ghosh, K. Gupta, A. Ghosh, U. Ghorai, A. Santra, P. Sasikumar and U. C. Ghosh, Efficiency evaluation of arsenic (III) adsorption of novel graphene oxide@ iron-aluminium oxide composite for the contaminated water purification, *Sep. Purif. Technol.*, 2018, **197**, 388–400.

87 X. Luo, C. Wang, L. Wang, F. Deng, S. Luo, X. Tu and C. Au, Nanocomposites of graphene oxide-hydrated zirconium oxide for simultaneous removal of As (III) and As (V) from water, *J. Chem. Eng.*, 2013, **220**, 98–106.